



HAL
open science

Panspermia in a Milky Way-like Galaxy

Raphael Gobat, Sungwook E. Hong, Owain Snaith, Sungryong Hong

► **To cite this version:**

Raphael Gobat, Sungwook E. Hong, Owain Snaith, Sungryong Hong. Panspermia in a Milky Way-like Galaxy. *The Astrophysical Journal*, 2021, 921, 10.3847/1538-4357/ac2829 . insu-03720853

HAL Id: insu-03720853

<https://insu.hal.science/insu-03720853>

Submitted on 12 Jul 2022

HAL is a multi-disciplinary open access archive for the deposit and dissemination of scientific research documents, whether they are published or not. The documents may come from teaching and research institutions in France or abroad, or from public or private research centers.

L'archive ouverte pluridisciplinaire **HAL**, est destinée au dépôt et à la diffusion de documents scientifiques de niveau recherche, publiés ou non, émanant des établissements d'enseignement et de recherche français ou étrangers, des laboratoires publics ou privés.



Distributed under a Creative Commons Attribution 4.0 International License



Panspermia in a Milky Way–like Galaxy

Raphael Gobat¹ , Sungwook E. Hong (홍성욱)^{2,3} , Owain Snaith⁴, and Sungryong Hong (홍성용)² ¹Instituto de Física, Pontificia Universidad Católica de Valparaíso, Casilla 4059, Valparaíso, Chile²Korea Astronomy and Space Science Institute, 776 Daedeok-daero, Yuseong-gu, Daejeon 34055, Republic of Korea; swhong@kasi.re.kr³Natural Science Research Institute, University of Seoul, 163 Seoulsiripdaero, Dongdaemun-gu, Seoul, 02504, Republic of Korea⁴GEPI, Observatoire de Paris, PSL Research University, CNRS, Place Jules Janssen, 92190, Meudon, France

Received 2021 July 21; revised 2021 September 2; accepted 2021 September 17; published 2021 November 11

Abstract

We study the process of panspermia in Milky Way–like galaxies by modeling the probability of successful travel of organic compounds between stars harboring potentially habitable planets. To this end, we apply the modified habitability recipe of Gobat & Hong to a model galaxy from the McMaster Unbiased Galaxy Simulations suite of zoom-in cosmological simulations. We find that, unlike habitability, which only occupies a narrow dynamic range over the entire galaxy, the panspermia probability can vary by orders of magnitude between the inner ($R, b = 1\text{--}4$ kpc) and outer disk. However, only a small fraction of star particles have very large values for the panspermia probability and, consequently, the fraction of star particles where the panspermia process is more effective than prebiotic evolution is much lower than from naïve expectations based on the ratio between the panspermia probability and natural habitability.

Unified Astronomy Thesaurus concepts: Exoplanet formation (492); Astrobiology (74); Habitable planets (695); Milky Way Galaxy (1054); Interstellar dust extinction (837); Galaxy stellar content (621)

1. Introduction

The notion that living organisms could travel between celestial bodies is almost as old as the concept of habitable worlds (e.g., Lucian’s *Vera Historia*, Kepler’s *Somnium*, or Voltaire’s *Micro-mégas*). Already present in embryonic form in some ancient mythologies, it was first formally named *panspermia* 25 centuries ago by the philosopher Anaxagoras. The development of microbiology in the 19th century opened up the possibility that such passage, rather than being directed, could take the form of the accidental propagation of simple *seeds* of life (e.g., Arrhenius & Borns 1908). This idea eventually spread through popular culture and became a minor staple of early 20th century speculative fiction, often playing on fears of invasion and contamination.

In the modern era of astrophysics, the concept of panspermia was famously embraced and developed by F. Hoyle and C. Wickramasinghe after the discovery of organic compounds in the interstellar medium (ISM) (e.g., Hoyle & Wickramasinghe 1977, 1978; Hoyle et al. 1983, 1986). Although never gaining widespread acceptance, likely due to a combination of practical and ideological factors (i.e., long odds and a perceived nonnecessity in explaining our world), panspermia has been the subject of a steady number of studies since then. It has experienced a resurgence lately with the discovery of multiple, possibly habitable, exoplanetary systems (Gillon et al. 2016; Zechmeister et al. 2019) and the recent crossing through the solar system of hyperbolic trajectory comets of probable interstellar origin (Meech et al. 2017; Higuchi & Kokubo 2019), starkly illustrating the possibility of matter exchanges between unbound star systems.

Modern studies involving panspermia broadly fall into three categories. The first concerns practical evaluations of the survivability of microorganisms to the various potentially lethal events that panspermia involves. Namely, their ejection from and

re-entry onto planetary surfaces (e.g., Melosh 1988; Burchell et al. 2001; Mastrapa et al. 2001; Burchell 2007; Stöffler et al. 2007; Price et al. 2013; Pasini & Price 2015) and transit through the harsh radiation environment of interplanetary and interstellar space (e.g., Weber & Greenberg 1985; Horneck et al. 1994; Secker et al. 1996; Horneck et al. 2001; Wickramasinghe & Wickramasinghe 2003; Yamagishi et al. 2018). These show that bacterial spores can survive hypervelocity impacts, as well as prolonged exposure to a combination of hard vacuum, low temperatures, and ionizing radiation. Although experiments were understandably not carried out over the timescales expected for interstellar panspermia, they nevertheless suggest that a small but not insignificant fraction of spores could survive the kiloyears or megayears of transit, especially when embedded in even a thin mantle of carbonaceous material.

The second type of study tries to estimate the timescale and types of mass transfer between planets orbiting a common host star, typically by the exchange of meteoroids (also called *lithopanspermia*; Wells et al. 2003; Gladman et al. 2005; Krijt et al. 2017; Lingam & Loeb 2017), or between stellar systems (e.g., Melosh 2003; Lingam & Loeb 2018), with the radiation pressure on small grains (also called *radio-panspermia*; Napier 2004; Wallis & Wickramasinghe 2004; Wesson 2010; Lingam & Loeb 2021). To these, we can also include speculations on the intentional seeding of other stellar systems via technological means (or *directed panspermia*; e.g., Crick & Orgel 1973).

The last category concerns statistical investigations of panspermic propagation through stellar systems or galaxies using analytical or simple numerical models (Adams & Spergel 2005; Lin & Loeb 2015; Lingam 2016; Ginsburg et al. 2018; Carroll-Nellenback et al. 2019; Đošović et al. 2019), or of the effect of a spatially variable probability of habitable planets (*habitability*; e.g., Gonzalez et al. 2001; Lineweaver et al. 2004; Gowanlock et al. 2011) on the viability of panspermia.

Here we couple the products of a hydrodynamical simulation of a Milky Way–like galaxy (Stinson et al. 2010; Nickerson et al. 2013) with a modified galactic habitability model (Gobat & Hong 2016, hereafter GH16) to investigate how the probability and



Original content from this work may be used under the terms of the [Creative Commons Attribution 4.0 licence](https://creativecommons.org/licenses/by/4.0/). Any further distribution of this work must maintain attribution to the author(s) and the title of the work, journal citation and DOI.

efficiency of panspermia vary with galactic environment. This paper is structured as follows: Sections 2 and 3 describe, respectively, the numerical simulation and habitability model that constitute the base of this study, while Section 4 presents the mathematical formalism we use for computing the probability of panspermia. We describe and discuss our results in Section 5 and summarize our conclusions in Section 6.

2. Simulation Data

The McMaster Unbiased Galaxy Simulations (MUGS) is a set of 16 simulated galaxies carried out by Stinson et al. (2010) and Nickerson et al. (2013). These simulations made use of the cosmological zoom method, which seeks to focus computational effort into a region of interest, while maintaining enough of the surrounding large-scale structure to produce a realistic assembly history. To accomplish this, the simulation was first carried out at low resolution using N -body physics only. Dark matter halos were then identified, and a sample of interesting objects selected. The particles making up, and surrounding, these halos were then traced back to their origin, and the simulation carried out again with the region of interest simulated at a higher resolution. The sample of galaxies was selected to have a minimal selection bias on the merging history or spin parameter. To be eligible for resimulation halos had to have a mass between 5×10^{11} and $2 \times 10^{12} M_{\odot}$, and be isolated for any object with a mass greater than $5 \times 10^{11} M_{\odot}$ by 2.7 Mpc. MUGS is therefore able to reproduce realistic infall and merging histories. Furthermore, they are able to reproduce the metallicity gradients seen in observed galaxies (e.g., Pilkington et al. 2012; Snaith et al. 2016), as well as features such as disks, halos, and bulges.

The MUGS galaxies were simulated in the context of a Λ CDM cosmology in concordance with the Wilkinson Microwave Anisotropy Probe 3 yr result (Spergel et al. 2007), with $(h, \Omega_m, \Omega_{\Lambda}, \Omega_b, \sigma_8) = (0.73, 0.24, 0.76, 0.04, 0.79)$. The simulations were carried out down to $z=0$ using the GASOLINE (Wadsley et al. 2004) smoothed-particle hydrodynamics code.

In the high-resolution region a gravitational softening length of 310 pc was used, with a hydrodynamical smoothing length of 0.01 times the softening length. The masses of the dark matter, gas, and stellar particles were 1.1×10^6 , 1.1×10^6 , and $6.3 \times 10^9 M_{\odot}$, respectively. In order to reproduce the baryonic properties of observed galaxies the simulations made use of ultraviolet (UV) background radiation, and metal-based cooling at low temperatures (Shen et al. 2010). These are based on results from CLOUDY (Ferland et al. 1998). To govern star formation, the simulations used a Schmidt–Kennicutt relation to relate the gas density to the star formation rate (SFR; Kennicutt 1998). This is further influenced by feedback processes from supernovae, which release energy and metals into the ISM (see Stinson et al. 2006 for details). A Kroupa initial mass function (IMF; Kroupa et al. 1993, hereafter KTG93) was used to calculate the stellar yields produced by each star particle.⁵ The slope of the IMF controls the ratio of high-mass to low-mass stars in a given simple stellar population (SSP), and each star particle is essentially an SSP. The effect of the fraction of high-mass stars is that it directly effects the ratio of oxygen to iron, because oxygen is produced by core-collapse supernovae, while iron is predominantly

produced by Type Ia supernovae (SNe Ia). Thus, the IMF affects the stellar yields from star particles.⁶ Metals are allowed to diffuse between gas particles, using the method outlined in Wadsley et al. (2008), in order to improve mixing.

We select one galaxy from MUGS for this study, g15784, which is characterized by a quiescent merger history. The galaxy has total and stellar masses of 1.5×10^{12} and $1.14 \times 10^{11} M_{\odot}$, respectively, and is therefore slightly larger than the Milky Way (Licquia & Newman 2015). g15784 has not experienced a merger with an object more massive than a 1:3 ratio since $z_{\text{imm}} \simeq 3.42$, similar to our own Galaxy (e.g., Stewart et al. 2008; Kruijssen et al. 2019; Naidu et al. 2021). Several spheroidal galaxies can be seen to orbit g15784 within 25 kpc of the galactic center (see Figure 1).⁷ For an overview of the detailed chemical properties of this galaxy, see Gibson et al. (2013) and Snaith et al. (2016), among other works.

Figure 2 shows the face-on radial profiles of the surface density, stellar age, and the metallicity of g15784. By taking the mean value of [Fe/H] in a series of radial bins between 3 kpc and 20 kpc we find this galaxy has a metallicity gradient of -0.012 dex kpc^{-1} . Outside of around 10 kpc the stars have a mean formation time of 6.5–7 Gyr, rising from a formation time of 3.6 Gyr at a 1.5 kpc. The SFR at $z=0$ is approximately $2.5 M_{\odot} \text{yr}^{-1}$. One important caveat is that the bulge-to-disk light ratio ($\log(B/D)$) for this galaxy is larger than expected for the Milky Way, reaching a value of -1.6 for g15784 (Brook et al. 2012), compared to $+0.14$ for the Milky Way (McMillan 2011). This is a known difference between the Milky Way and MUGS galaxies (Stinson et al. 2010; Allen et al. 2006). This is the effect of insufficient feedback and resolution to capture all the physical processes required to produce a realistic simulated galaxy.

From now on, we only consider the star particles located between 1–25 kpc from the mass-weighted center of the g15784. We ignore the inner 1 kpc since it is not well resolved. We find a massive knot of particles in the inner few softening lengths, and the high stellar and gas density of this region might thus be an artifact of the simulation (Stinson et al. 2010). The volume we consider contains 977,304 star particles, which we separate into three distinct regions: (1) the `CentralDisk`, located in galactocentric radius $R=1\text{--}4$ kpc with a thickness of 1 kpc along the galactic plane; (2) the `DiskHalo`, which corresponds to both the inner disk ($R=1\text{--}4$ kpc with larger thickness than `CentralDisk`), outer disk ($R=4\text{--}20$ kpc), and galactic halo outside the disk; and (3) the `Spheroids` that include two orbiting spheroids.

3. Levels of Habitability

For each $6.3 \times 10^6 M_{\odot}$ star particle, we compute a measure of *habitability*, that is, the fraction of main-sequence low-mass stars with terrestrial planets within their habitable zones (HZs). We mostly follow the model described in GH16 and refer to that paper for more details on its various components. A quick summary of its formalism is as follows. The habitability fraction f_{hab} of a given star particle at the time $t=t_z$ is defined

⁵ It is important to remember that each star particle is an ensemble of stars with a range of masses but the same metallicity. This is a consequence of the resolution limits of simulations, which cannot follow individual stars through time.

⁶ Pilkington et al. (2012) found that the metallicity, Z , is calculated as $O + Fe$, meaning that it is 1.8 times lower than expected. This may have a small impact on the cooling rate of gas, etc.

⁷ For more details see <https://mugs.mcmaster.ca/g15784.html>.

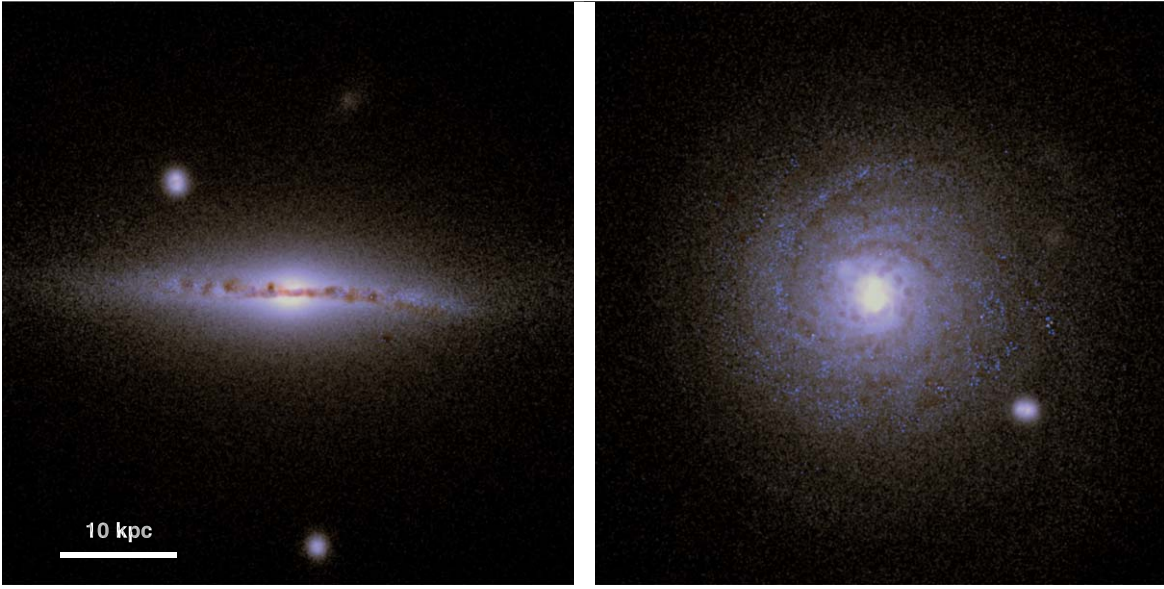


Figure 1. Mock *UVJ* color images of the simulated galaxy $g15784$ (Stinson et al. 2010; Nickerson et al. 2013), for both edge-on (left) and face-on (right) orientations, using star and gas particles, and assuming Bruzual & Charlot (2003) stellar population models and a simple dust attenuation model (Li & Draine 2001) with a gas-to-dust ratio of 0.01 at solar metallicity. Additionally, we include line emission from star particles with ages ≤ 50 Myr, following *case B* recombination (Osterbrock & Ferland 2006) and metallicity-dependent line ratios (Anders et al. 2003). All panels are 50 kpc across and have a resolution of 100 pc. Two spheroidal satellites can be seen above and below the galactic plane, respectively.

as

$$f_{\text{hab}} = \frac{1}{n_{\star}} \int_0^{t_z - t_{\text{min}}} dt (1 - V_{\text{irr}}) \Psi \times \int_{m_{\text{min}}}^{1.5 M_{\odot}} dm m \phi \mathcal{H}(t_{\text{MS}} - t) w_{\text{h}}, \quad (1)$$

with

$$n_{\star}(t_z) = \int_0^{t_z} dt \Psi \int_{m_{\text{min}}}^{m_{\text{max}}} dm m \phi \mathcal{H}(t_{\text{MS}} - t) \quad (2)$$

$$w_{\text{h}}(m, Z, t) = f_{\text{T}} \mathcal{H}(1.5 M_{\odot} - m) \times \left(\int_{r_{\text{h},i}}^{r_{\text{h},o}} dr P^{\beta_p} \frac{dP}{dr} \right) / \left(\int dr N \frac{dP}{dr} \right) \quad (3)$$

$$f_{\text{T}}(Z) = \mathcal{H}(Z - Z_{\text{min}}) \left[f_{\text{T},0} - f_{\text{HJ}} \left(\frac{Z}{Z_{\odot}} \right)^{\alpha_p} \right], \quad (4)$$

where $\mathcal{H}(x)$ is the Heaviside step function, and $(m_{\text{min}}, m_{\text{max}}) = (0.1 M_{\odot}, 100 M_{\odot})$ are the minimum and maximum mass of a star, respectively. $\Psi(t)$ is the star particle's star formation history (SFH),⁸ $\phi(m)$ is its IMF, and $V_{\text{irr}}(t)$ is its (time-dependent) volume fraction irradiated by SNe. $t_{\text{MS}}(m, Z)$ is the main-sequence lifetime of a star with mass m and metallicity Z , and $r_{\text{h},i}(m, Z, t)$ and $r_{\text{h},o}(m, Z, t)$ are the inner and outer radii of its HZ, respectively. $P(r, m)$ are the orbital periods of planets orbiting that star, whose distribution follows a simple power law $dN \propto P(r, m)^{\beta_p} dP$ (e.g., Cumming et al. 2008; Petigura et al. 2013; Burke et al. 2015). $f_{\text{T}}(Z)$ is the fraction of stars with terrestrial planets (*Case 2* of the metallicity dependence in GH16), and f_{HJ} is the fraction of solar-metallicity stars with

short-period gas giants (hot Jupiters), with $Z_{\text{min}} = 0.1 Z_{\odot}$ being a metallicity threshold below which we assume that terrestrial planets cannot form. We do not consider the contribution of the active nucleus in the galactic core, since the distance at which its additional radiative input significantly alters HZs is somewhat smaller (GH16) than the radius of the simulation volume we ignore. The number of (potentially) habitable stellar systems in each star particle is therefore given as $n_{\text{hab}} = f_{\text{hab}} n_{\star}$.

The values of each parameter we used in this paper are the same as in GH16: $(f_{\text{HJ}}, \alpha_p, \beta_p) = (0.012, 2, -0.7)$, with the following exceptions. First, t_{min} , the time after which a planet is considered able to host life, is decreased from 1 Gyr to 500 Myr in the *natural* case (see below). Also, we set $f_{\text{T},0} = 1$ (similar to Zackrisson et al. 2016) to reconcile the predictions of the model with Kepler constraints (He et al. 2019), which previously differed by a factor of ~ 2 (GH16). Finally, we modify the inner radius of the HZ (Equation (3) in Kopparapu et al. 2013), to account for increased flare activity in low-mass stars. In essence, we increase the luminosity L of every star by the energy-integrated cumulative distribution of flare frequency (which we approximate as a power law with an index of -0.8), limited by its mass-dependent maximum flare energy, from Davenport (2016). Since we are only concerned with average quantities, we simply weigh this additional luminosity by the fraction of flaring stars to derive the fractional increase per stellar mass. This has the effect of slightly reducing the habitability weight $w_{\text{h}}(m, Z, t)$ of sub-solar-mass stars. However, the effect is mild enough that it does not modify our results.⁹

We compute supernova rates (SNR) for each star particle based on its SFH and neighboring particles at each time step, using simulation snapshots from $z = 10.8$ to $z = 0$, spaced by

⁸ Since star particles are created just once due to the construction of the numerical simulation, this simply corresponds to a delta burst, to which we assign a duration of 100 Myr.

⁹ In a similar way, atmospheric erosion by intense stellar winds might also push the inner edge of the HZ outwards without impacting its outer radius (e.g., see Dong et al. 2018), effectively narrowing it further around M dwarfs as they age.

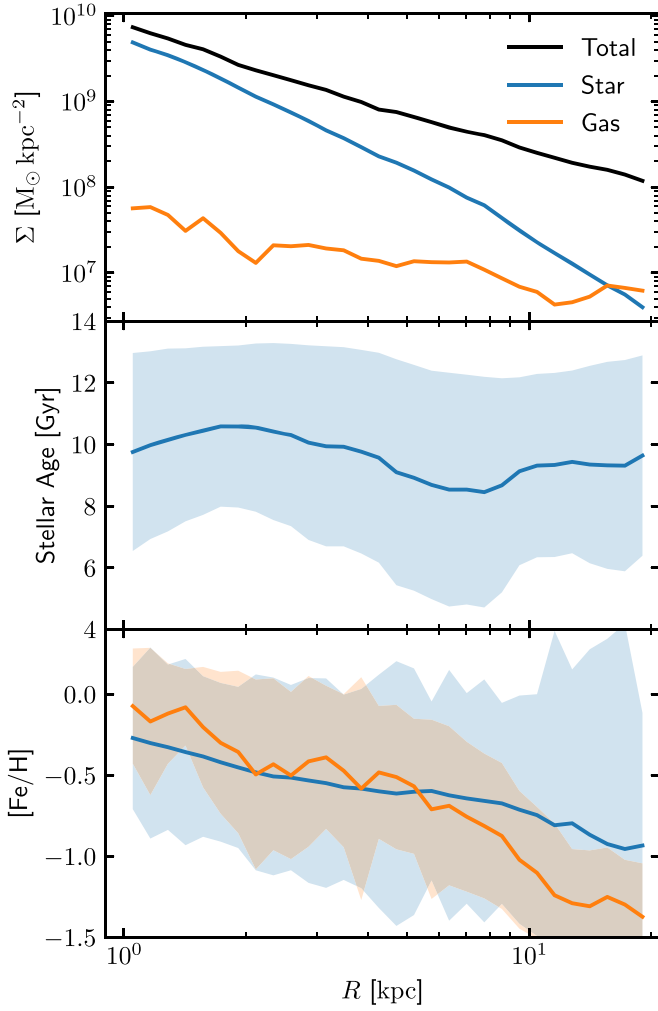


Figure 2. Face-on radial profiles of the surface density (top), stellar age (middle), and the metallicity (bottom) of g_{15784} at $z=0$. Shaded regions show the standard deviation within a given radial bin.

~ 200 Myr. We consider SNe Ia and II, with

$$\text{SNR}_{\text{Ia}}(t) = \eta_{\text{WD}} \int_{m_{\text{min}}}^{8 M_{\odot}} dm m \times \int_{\tau_{\text{Ia}} + t_{\text{MS}}(8 M_{\odot})}^t dt' \Psi(\tau) \phi(m, \tau), \quad (5)$$

$$\text{SNR}_{\text{II}}(t) = \Psi(t) \int_{8 M_{\odot}}^{m_{\text{max}}} dm m \phi(m, t), \quad (6)$$

where $\eta_{\text{WD}}=0.01$ is the white dwarf (WD) conversion rate (Pritchett et al. 2008), $\tau = t' - t_{\text{MS}}(m) - \tau_{\text{Ia}}$, and $\tau_{\text{Ia}} = 500$ Myr is the average delay time between stellar death and the detonation of the WD (Raskin et al. 2009). An example of SNRs for selected star particles in g_{15784} is given in Figure 3. The volume irradiated by SNe within star particle i is then

$$V_{\text{irr},i}(t) = \frac{\mathcal{H}(t_{\text{rec}} - t)}{r_p^3} \times \sum_j v_{ij} (\text{SNR}_{\text{Ia},j} r_{\text{Ia}}^3 + \text{SNR}_{\text{II},j} r_{\text{II}}^3), \quad (7)$$

where $(r_{\text{Ia}}, r_{\text{II}}) = (0.3 \text{ pc}, 0.5 \text{ pc})$ are the lethal radii of SNe Ia and II, respectively (GH16). v_{ij} is the fractional volume where

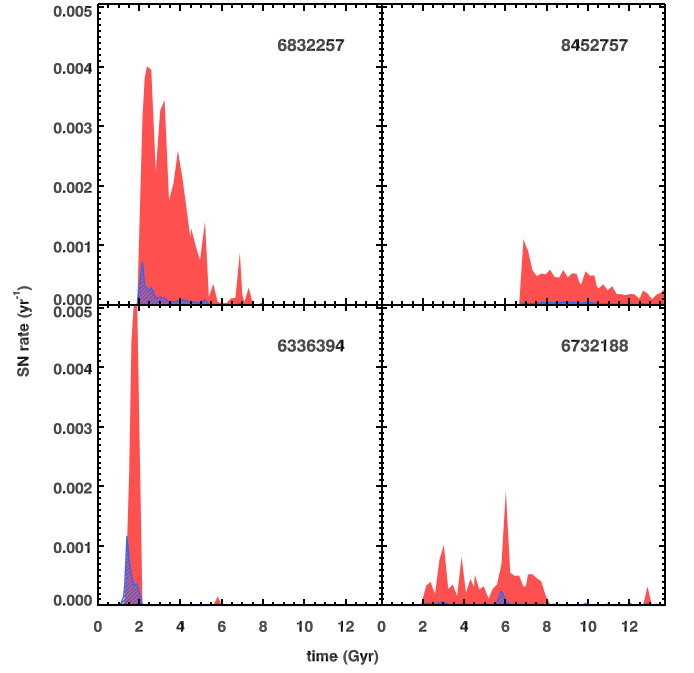


Figure 3. Rates of Type Ia (red) and Type II (blue) SNe for selected star particles in g_{15784} . Particle IDs are shown in the upper right corner of each panel.

the two $6.3 \times 10^6 M_{\odot}$ particles overlap (with $v_{ii} = 1$), computed assuming that each corresponds to a spherical volume of radius r_p , set by the gravitational softening length, homogeneously filled with stars. As in GH16, the recovery time t_{rec} is set to an arbitrarily large value so that V_{irr} is always positive.

In a majority of cases, most of the SNR felt by individual star particles is contributed by neighboring particles, whose volumes overlap each other. This, together with their higher metallicity (to which $f_{\text{T}}(Z)$ is anticorrelated), reduces the habitability of star particles within the crowded galactic bulge, as shown in Figure 4. On the other hand, the higher density and SNRs found in spiral arms have little effect, although a smattering of low-habitability particles exists in these regions. The average f_{hab} of the disk reaches a (weak) maximum at $\sim 4\text{--}5$ kpc from the center (Figure 5), decreasing smoothly further out due to an increased fraction of very low-metallicity $f_{\text{hab}}=0$ star particles. This behavior is somewhat similar to the model of Lineweaver et al. (2004) but in contrast with the radially monotonous trend from Gowanlock et al. (2011). The galactic halo similarly contains a mix of lower- and higher-habitability star particles, with a significant fraction of $< 0.1 Z_{\odot}$ nonhabitable star particles and a slightly lower average f_{hab} than the disk.

Overall, we find that the range of positive f_{hab} is somewhat narrow at $z=0$, with most particles having values within $\sim 5\%$ of each other, which is similar to Prantzos (2008). This is not entirely surprising since the probability of terrestrial planets f_{T} is, in this model, only weakly correlated with metallicity and the effect of supernovae on habitability is not strong (GH16). However, the variation increases by order of magnitude at $z > 0.5$, due to a significantly higher number of star particles below the $0.1 Z_{\odot}$ threshold (especially at large galactocentric radii) and a much higher SNR (especially in the core).

Finally, we consider two other levels of habitability in addition to the *natural* criterion described above, where a planet is deemed habitable quickly and SN effects are small. These are intended to

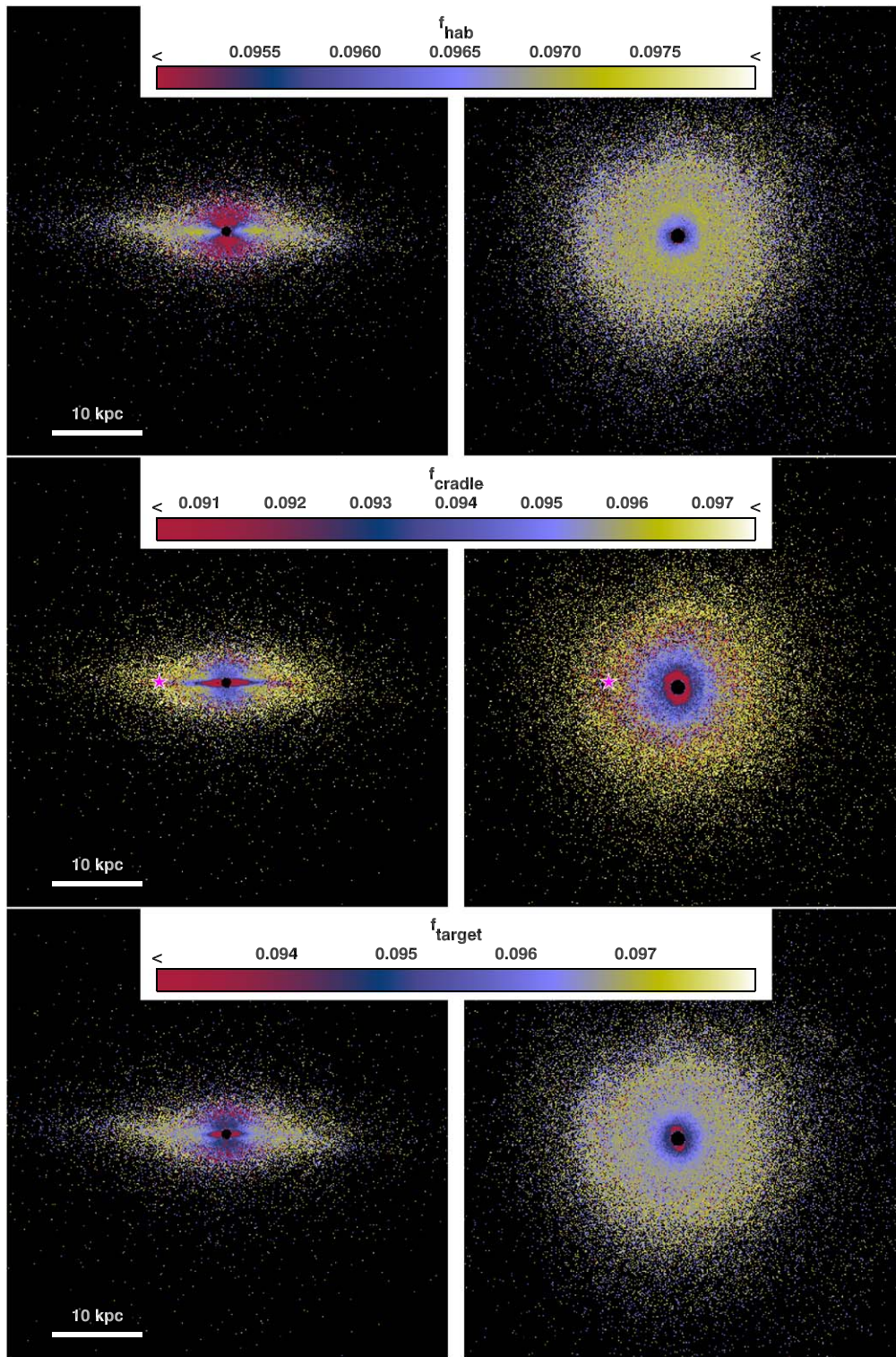


Figure 4. Similar to Figure 1, except showing the median value of the *natural* habitability (f_{hab} ; top), the fraction of possible *cradles* (f_{cradle} ; middle), and the fraction of possible colonization *targets* (f_{target} ; bottom) within each projected column at $z=0$ and in a 1 kpc wide slice passing through the center of g15784. The magenta star corresponds to the approximate position of the Sun, if it were the actual Milky Way.

better describe the fraction of planets where life could arise or take hold (see Section 4.1), as opposed to the larger population with just benign surface conditions. The first habitability level is meant to mirror the present state of the Earth, where we set $t_{\text{min}} = 4.5$ Gyr and require that no SNe happened within $r_{\text{Ia}} = r_{\text{II}} = 8$ pc of planets in the last $t_{\text{rec}} = 50$ Myr. We regard this habitability level, f_{cradle} , as describing the *cradles* of potential

civilizations, that is, the origin point of directed panspermia. Also, we consider a less restrictive case, with $t_{\text{min}} = 1$ Gyr and $t_{\text{rec}} = 1$ Myr, to describe the potential *targets* of such directed panspermia (f_{target}). The requirement for a small but nonzero t_{rec} also allows us to sidestep the issue of transit of organisms through the radiation environment of supernova remnants. Contrarily to the natural case, here the low-habitability star particles are

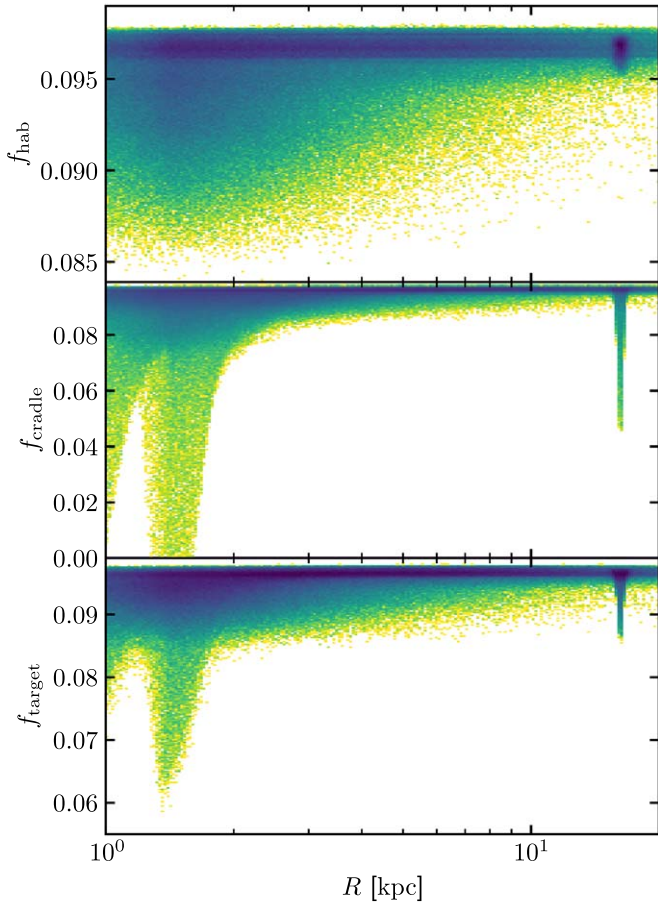


Figure 5. The fraction of *natural* habitable planets (f_{hab} ; top), *cradles* of potential civilizations (f_{cradle} ; middle), and possible colonization *targets* (f_{target} ; bottom), as a function of galactocentric radius in g_{15784} at $z=0$, drawn in a logarithmic scale.

concentrated within the `CentralDisk`, up to ~ 4 kpc as shown in Figures 4 and 5, due to the higher SN efficiency at suppressing habitability. The outer galactic disk also has lower averages of f_{cradle} and f_{target} , due to the higher prevalence of recently formed star particles, and the distributions of cradles and targets are similar.

4. Modeling the Probability of Panspermia

The probability that seeds of life departed from star particle i at position \mathbf{x}_i at time t_i (hereafter, (\mathbf{x}_i, t_i)) to be successfully transplanted to star particle j at (\mathbf{x}_j, t_j) can be written as

$$\begin{aligned} \mathcal{F}(\mathbf{x}_i, t_i; \mathbf{x}_j, t_j) &= f_{\text{oc}}(\mathbf{x}_i, t_i) f_{\text{target}}(\mathbf{x}_j, t_j) f_{\text{esc}}(\mathbf{x}_i) f_{\text{cap}}(\mathbf{x}_j) \\ &\times \int_{\mathbb{V}_i} d\mathbf{x}'_i \int_{\mathbb{V}_j} d\mathbf{x}'_j w_{\text{damage}}(\mathbf{x}'_j, t_j | \mathbf{x}'_i, t_i). \end{aligned} \quad (8)$$

The definitions of f_{oc} , f_{target} , f_{esc} , f_{cap} , and w_{damage} are given progressively in the following sections. We note that, while here we apply Equation (8) to what are effectively groupings of millions of stars, it can also be used to describe panspermia between two individual stars. Then the total amount transplanted to a star particle at (\mathbf{x}_j, t_j) is proportional to

$$f_{\text{pp}}(\mathbf{x}_j, t_j) = \sum_{\mathbf{x}_i} \int_0^{t_j} dt_i \mathcal{F}(\mathbf{x}_i, t_i; \mathbf{x}_j, t_j). \quad (9)$$

We hereafter call \mathcal{F} and f_{pp} the *panspermia contribution* and *panspermia probability*, respectively.¹⁰ While t_j should always be greater than t_i , \mathbf{x}_i and \mathbf{x}_j can be the same since a single star particle in our analysis contains millions of stars.

4.1. Probability of Hosting Life

First, $f_{\text{oc}}(\mathbf{x}_i, t_i)$ is the probability that the star particle i has planets bearing living organisms, or their complex organic precursors, at t_i . For a star particle having these seeds, it should be habitable for a period sufficient for successful prebiotic evolution. This can be written as

$$f_{\text{oc}}(\mathbf{x}, t) = \int_{t-t_{\text{chem}}}^t dt' f_{\text{hab}}(\mathbf{x}, t') W_{\text{chem}}(t-t'), \quad (10)$$

where $t_{\text{chem}} \sim \mathcal{O}(10^{-1} \text{ Gyr})$ is the typical timescale for prebiotic evolution (Mojzsis et al. 1996; van Zuilen et al. 2002; Dodd et al. 2017), and W_{chem} is a certain time-domain kernel between f_{hab} and f_{oc} , respectively. In practice, as W_{chem} is unknown and t_{chem} is much smaller than timescales used in this paper (e.g., timescales for star formation, local SN rates, and delay time for f_{hab}). Therefore, for simplicity, we assume that the probability of hosting life is similar to the fraction of possible *cradles* of life, that is, $f_{\text{oc}}(\mathbf{x}, t) \propto f_{\text{cradle}}(\mathbf{x}, t)$.

4.2. Escape Fraction

$f_{\text{esc}}(\mathbf{x}_i)$ is a weight proportional to the escape fraction of life spores, from habitable planets in the star particle i to the ISM by natural processes. In order to estimate f_{esc} in the case of natural panspermia, we assume that material carrying spores can be ejected from the surface of habitable terrestrial planets by surface impacts. The velocity of ejecta is (Housen & Holsapple 2011)

$$v_{\text{ej}} = u \cdot C_1 \left[\frac{x}{a_e} \left(\frac{\rho}{\delta} \right)^\nu \right]^{-\frac{1}{\mu}} \left(1 - \frac{x}{n_2 R} \right)^{n_2} \quad (11)$$

at a distance x from the impact center, with $n_1 a \leq x \leq n_2 R$, where R is the radius of the impact crater, and u the impactor's velocity, which we assume to be equal to the average orbital velocity $v_{\text{orb, HZ}}(m_*)$ within the star's HZ.¹¹ For Equation (11), we use parameter values for low-porosity rock given in Housen & Holsapple (2011), namely, $\mu = 0.55$, $\nu = 0.4$, $C_1 = 1.5$, $n_1 = 1.2$, $n_2 = 1$, $p_e = 0.5$, $\rho/\delta \sim 1$, and $a_e = 0.0016$. The radius R of the crater is related to the impactor's energy through

$$\frac{R}{\text{km}} \sim \frac{1}{2} \left(\frac{E_{\text{kin}}}{9.1 \times 10^{24} \text{ erg}} \right)^{1/2.59} \quad (12)$$

(Hughes 2003), where $E_{\text{kin}} = \frac{1}{2} m_i v_{\text{orb, HZ}}^2$, with m_i being the mass of the impactor. Assuming that the latter follows a distribution of the type $\propto m^{-1.6}$ (Simon et al. 2017), we can then compute a velocity distribution of ejecta (see Figure A1).

¹⁰ The actual probability that the panspermia process is successful may not be simply additive as assumed in Equation (9), but this is beyond the scope of this paper.

¹¹ The typical velocity of impactors may actually be closer to half of the planet's orbital velocity (e.g., see Collins et al. 2005), which would naturally decrease the number of fragments reaching escape velocity. However, this would not change the "normalized" value of the escape weight f_{esc} which we use here.

Only a small fraction of the ejected material will have enough velocity to escape the planet and thus only an infinitesimal quantity of this material can ever reach stellar escape velocity in the simulation. On the other hand, we can expect that a fraction w_{esc} of material ejected into circumstellar orbit can be accelerated above stellar escape velocity by either gravitational interactions (in the case of macroscopic fragments, which corresponds to lithopanspermia; Melosh 1988) or radiation pressure (in the case of microscopic fragments; Arrhenius & Borns 1908). Under the assumption that the host-star mass does not determine the magnitude and frequency of these boosts, w_{esc} is only a function of orbital and stellar escape velocities within the HZ:

$$w_{\text{esc}}(m) = C \int_{r_{h,i}(m)}^{r_{h,o}(m)} \int_{v_{\text{esc}}(r)} \phi_{\text{ej}}(v) dv dr, \quad (13)$$

where ϕ_{ej} is the quantity of ejected material as a function of velocity (see Figure A1) and C is a normalizing constant. Following this scheme, w_{esc} would be higher for higher-mass stars (Figure A1), as the radius of the HZ increases with $L^{1/2}$ (that is, with $\sim M^{1.75}$). The same applies to lower-metallicity stars, which are brighter for the same mass. Since the magnitude and frequency of the boosts are unknown, a quantitative estimate for w_{esc} is however not possible. Instead, we compute relative quantities, rescaled to an arbitrary range of $[0, 1]$ for our star particles at $z=0$. Integrating this over the age-truncated KTG93 IMF then yields a weight

$$f_{\text{esc}}(t) = \int d \log m \phi(m, t) w_{\text{esc}}(m) N_{\text{impact}}(t) \quad (14)$$

for each star particle. Here we assume for simplicity that w_{esc} does not vary with the age of the stellar particle. However, we note that the frequency of impacts on Earth has decreased exponentially since the formation of the solar system, which would result in a time-varying f_{esc} . Since w_{esc} depends on the position of the HZ, the spatial distribution of f_{esc} within $\mathfrak{g}15784$ is similar to f_{hab} (Figures 4 and 5), being low within the CentralDisk, reaching a maximum at ~ 5 kpc, and monotonously decreasing at larger galactocentric radii. For a more detailed description, see Appendix A.

4.3. The Capture Fraction

$f_{\text{cap}}(\mathbf{x}_j)$ is the capture fraction of interstellar spores by target planets in the star particle j by gravity. Here, we assume that stars are evenly distributed in each star particle, and that each star is separated from the others by a distance much greater than the size of its planetary system.

The probability of interstellar objects captured by solar systems can be sensitive to the structure of planetary systems (e.g., Ginsburg et al. 2018). However, this fine structure lays considerably beyond the resolution of the simulation used here. Consequently, and for convenience, we assume $f_{\text{cap}}(\mathbf{x}_j)$ to be simply constant on average.

4.4. Traveling Seeds

The last term of Equation (8) corresponds to the probability that spores originating from a habitable planet within the star particle i (\mathbb{V}_i) at t_i reach a target planet within the star particle j (\mathbb{V}_j) at t_j . Mathematically, it is calculated as the double volume integral of $w_{\text{damage}}(\mathbf{x}'_j, t_j | \mathbf{x}'_i, t_i)$, the survival probability of spores in an

interstellar object that starts at (\mathbf{x}'_i, t_i) and arrives (\mathbf{x}'_j, t_j) (hereafter, the *damage weight*), where $\mathbf{x}'_{i,j} \in \mathbb{V}_{i,j}$. To compute this numerically, one needs to understand the spatial distribution of stars in each star particle, as well as consider the traveling distance (ℓ_{surv}), which is a function of the survival timescale of spores in the ISM (t_{surv}), and how w_{damage} depends on ℓ_{surv} .

As mentioned in Section 2, each star particle in $\mathfrak{g}15784$ is an ensemble of millions of stars whose total mass is about $6.3 \times 10^6 M_{\odot}$. While the volume of such an ensemble can be approximated by the cell from the Voronoi tessellation¹² of star particles, the actual distribution of stars within the volume is unknown. Here we assume that the stars in a star particle are uniformly distributed in its Voronoi volume by adopting such numerical limitation. Furthermore, for a fast calculation of the panspermia probability, we simplify the geometry of the star particle i to a sphere with center at \mathbf{x}_i and radius $R_i \equiv (3V_i/4\pi)^{1/3}$, where V_i is its Voronoi volume. Such assumptions will work well for small-volume star particles at a relatively dense region of $\mathfrak{g}15784$ because the stellar density gradient within the volume will be low, and the shape of the Voronoi cell will be close to the sphere due to numerous nearby cells. On the other hand, our assumptions may work poorly for star particles at the outskirts of $\mathfrak{g}15784$. However, these typically do not contribute much to our main results because of their low habitability and panspermia probability.

The survival time of microorganism spores under the pressures, temperatures, and radiation flux expected for panspermia is uncertain. All in situ experiments so far have been done in Earth orbit (e.g., Horneck et al. 2001; Onofri et al. 2012; Kawaguchi et al. 2013) and their conclusions are typically extrapolated to the requirements for in-system panspermia (e.g., between the Earth and Mars). On the other hand, they do not reflect the likely conditions of interstellar panspermia; in particular, the survival of spores under hard radiation has been found to increase at low temperatures (Weber & Greenberg 1985; Sarantopoulou et al. 2011). Only a few biological studies concerning an interstellar transit have been carried out (Weber & Greenberg 1985; Koike et al. 1992; Secker et al. 1994), which suggest that shielding by a rock or carbonaceous material would be required to ensure the survival of a sufficient number of spores. With no clear constraints on the survival timescale, we assume a conservative choice of $t_{\text{surv}} \sim \mathcal{O}(1 \text{ Myr})$. For simplicity, we also assume that t_{surv} is negligible compared to the evolution timescale of the Milky Way so that we can use the characteristics of star particles from the snapshot data at $z=0$ for both t_i and t_j .

The survival timescale t_{surv} can be rewritten in terms of the travel distance scale $\ell_{\text{surv}} \equiv \bar{v}_{\text{oc}} t_{\text{surv}}$, where \bar{v}_{oc} is the mean velocity of the spores. As already discussed in Section 4.3, the distance between different solar systems is much larger than the typical size of a solar system. Therefore, we assume that, although not exactly zero, the probability that interstellar objects would significantly change their trajectories or speed due to the gravity from a single solar system when they are in the middle of the ISM is low. Here we adopt the velocity of comet 'Oumuamua ($26.32 \pm 0.01 \text{ km s}^{-1}$; Mamajek 2017) as typical of \bar{v}_{oc} for rocky objects crossing the ISM. While the speed of interstellar objects may depend on their distance from

¹² Voronoi tessellation partitions a volume into multiple regions, based on a set of positions $\{\mathbf{x}_i\}$. The Voronoi volume of a particle \mathbf{x}_i is then defined as an ensemble of points whose closest particle is \mathbf{x}_i , that is, $\mathbb{V}_i \equiv \{\mathbf{x} | |\mathbf{x}, \mathbf{x}_i| < |\mathbf{x} - \mathbf{x}_j| \text{ for all } j \neq i\}$.

the galactic center, we do not consider it here for simplicity. Combining t_{surv} and \bar{v}_0c yields a typical scale ℓ_{surv} of a few parsecs, which matches well with the estimation of $\ell_{\text{surv}} = 15\text{--}30$ pc in Grimaldi et al. (2021). In the following section, we use a range of $\ell_{\text{surv}} = 1\text{--}10^4$ pc to explore the parameter space and account for simple cases of *directed* panspermia (e.g., in the case of $\ell_{\text{surv}} \gtrsim 1$ kpc; see also Stapleton 1930; Haldane 1954; Crick & Orgel 1973), while keeping in mind that $\ell_{\text{surv}} \leq 30$ pc is likely more appropriate to the *natural* case.

As the dependency of the damage weight w_{damage} to the travel distance $\ell \equiv |\mathbf{x}'_i - \mathbf{x}'_j|$ ($\mathbf{x}'_{i,j} \in \mathbb{V}_{i,j}$) is not precisely known, we consider three different models for w_{damage} : (1) a *sudden* damage model (*sudden* hereafter), where spores stay alive at $\ell < \ell_{\text{surv}}$ and suddenly die afterward; (2) a *linear* damage model (*lin* hereafter), in which the population linearly decreases over time until it becomes zero at $\ell = \ell_{\text{surv}}$; and (3) an *exponential* damage model (*exp* hereafter), where the population of viable spores exponentially decreases over time, assuming that the survival rate over a fixed time period is constant:

$$w_{\text{damage}}\left(\frac{\ell}{\ell_{\text{surv}}}\right) = \begin{cases} \mathcal{H}(1 - \ell/\ell_{\text{surv}}) & (\text{sudden}) \\ \max\{1 - \ell/\ell_{\text{surv}}, 0\} & (\text{lin}) \\ \exp(-\ell/\ell_{\text{surv}}) & (\text{exp}) \end{cases} \quad (15)$$

Finally, we also consider a fourth damage model, *noEsc*, which is identical to *sudden* where $f_{\text{esc}} = 1$ for all star particles, in order to understand the dependency of the panspermia probability on f_{esc} . We also note that, unlike *sudden* and *lin*, 37% of the spores are still alive at $\ell = \ell_{\text{surv}}$ in *exp*. Therefore, one should be careful when comparing the dependency of the panspermia probability on ℓ_{surv} between *exp* and others.

4.5. Numerical Formalism

Summarizing the above subsections, one can rewrite Equations (8) and (9) as follows:

$$f_{\text{pp}}(\mathbf{x}_j) = \sum_i \mathcal{F}(\mathbf{x}_i, \mathbf{x}_j), \quad (16)$$

where

$$\mathcal{F}(\mathbf{x}_i, \mathbf{x}_j) \propto f_{\text{cradle}}(\mathbf{x}_i) f_{\text{esc}}(\mathbf{x}_i) f_{\text{target}}(\mathbf{x}_j) \times \int_{\ell_{\text{min}}}^{\ell_{\text{max}}} d\ell F(\ell|R_i, R_j, D_{ij}) w_{\text{damage}}\left(\frac{\ell}{\ell_{\text{surv}}}\right). \quad (17)$$

Since all timescales in Equations (8) and (9) are smaller than the dynamic timescale of the galaxy, we neglect time-dependent terms in the original equations. Here, $D_{ij} \equiv |\mathbf{x}_i - \mathbf{x}_j|$ is the distance between the centers of two star particles, considered as volumes homogeneously filled with stars. Also, $\ell_{\text{min}} \equiv \max\{0, D_{ij} - R_i - R_j\}$ and $\ell_{\text{max}} \equiv \min\{\alpha_{\text{trunc}} \ell_{\text{surv}}, D_{ij} + R_i + R_j\}$ are the minimum and maximum values of ℓ during the integration, respectively. A truncation rate α_{trunc} is defined as the minimum value that satisfies $w_{\text{damage}}(\alpha_{\text{trunc}}) = 0$, whose value is 1 for *sudden* and *lin*. For *exp*, we manually set $\alpha_{\text{trunc}}^{\text{exp}} \gg 1$ for a fast calculation.

$F(\ell|R_i, R_j, D_{ij})$ is the probability of having $|\mathbf{x}'_i - \mathbf{x}'_j| = \ell$ given R_i, R_j , and D_{ij} , and assuming that the timescale for

panspermia is much less than the evolution timescale of the galaxy:

$$F(\ell|R_i, R_j, D_{ij}) = \frac{3}{R_i^3} \int dD D^2 f_{\text{sp}}(D|D_{ij}, R_i) f_{\text{sp}}(\ell|D, R_j), \quad (18)$$

where

$$f_{\text{sp}}(d|D, R) = \begin{cases} 0 & \text{at } d > D + R \\ \mathcal{H}(R - D) & \text{at } d < |D - R| \\ \frac{R^2 - (d - D)^2}{4Dd} & \text{otherwise} \end{cases} \quad (19)$$

is the fraction of a spherical surface with radius d that belongs to the volume of another sphere of radius R at distance D .

From Equation (16), one can also estimate a probability that seeds spreading from a given star particle are successfully transplanted in another (hereafter, the *successful transplantation probability*):

$$f_{\text{stp}}(\mathbf{x}_i) = \sum_j \mathcal{F}(\mathbf{x}_i, \mathbf{x}_j). \quad (20)$$

Since several factors in Equations (8) and (9) remain unknown, Equations (16) and (20) thus only yield relative, rather than absolute, values of the panspermia probability. However, since our main focus is a relative comparison between habitability and panspermia probability, we hereafter normalize f_{pp} and f_{stp} so that their sum over $\mathfrak{g}15784$ is same to the sum of the habitability, that is,

$$\sum_{\mathbf{x}} f_{\text{pp}}(\mathbf{x}) = \sum_{\mathbf{x}} f_{\text{stp}}(\mathbf{x}) = \sum_{\mathbf{x}} f_{\text{hab}}(\mathbf{x}). \quad (21)$$

5. Results

5.1. Panspermia Probability and Successful Transplantation Probability

Figures 6–8 show the spatial and probability distributions of the panspermia probability and successful transplantation probability in $\mathfrak{g}15784$ at $z = 0$, normalized following Equation (21). Similarly to the three habitability levels, star particles in the *CentralDisk* have very low f_{pp} and f_{stp} . In the *DiskHalo* region, both f_{pp} and f_{stp} tend to have higher values at a lower galactocentric radius (R) and tangential distance from the galactic plane (b). However, while f_{pp} covers a wide range of 7 orders of magnitude and shows a somewhat mixed distribution at $R > 5$ kpc, the successful transplantation probability f_{stp} shows a narrower range (3 orders of magnitude) and stronger dependency on both R and b , in the $\ell_{\text{surv}} = 100$ pc case. For larger values of ℓ_{surv} , however, f_{pp} tends to show a stronger negative slope in a R -direction (upper panel of Figure 7). Such a negative slope at high ℓ_{surv} might happen because of the difference, between low R (high Σ_*) and high R (low Σ_*), in the number of sources that a given star particle can receive.

The probability distribution of $p(f_{\text{pp}})$ peaks at around 10^{-4} times the typical value of the habitabilities. As the travel distance increases, the peak of $p(f_{\text{pp}})$ shifts toward lower values, decreases, and widens. This is because a large ℓ_{surv} allows seeds to reach distant star particles, which naturally increases the total amount of successfully transplanted seeds in a given galaxy. However, since we normalize f_{pp} so that its sum over the galaxy is constant, the importance of each successfully

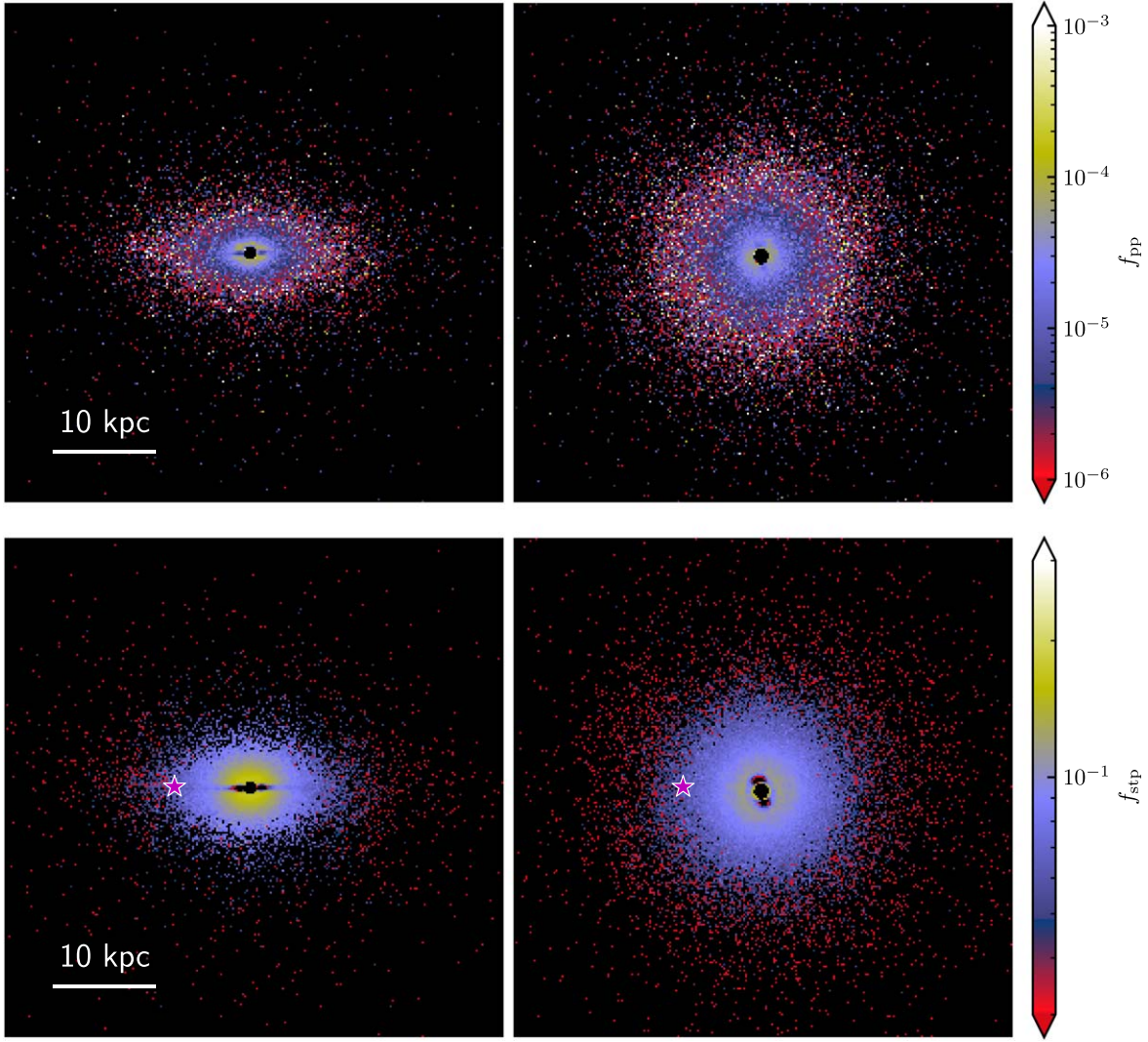


Figure 6. Panspermia probability (f_{pp} ; top) and successful transplantation probability (f_{stp} ; bottom) at $z=0$ in $g15784$, assuming the exponential damage model (exp) with $\ell_{surv} = 100$ pc. The field of view, slice width, and the magenta star are set to be the same as Figure 4.

transplanted seed decreases. On the other hand, the peak position of the probability distribution of normalized successful transplantation probability ($p(f_{stp})$) remains similar regardless of the value of ℓ_{surv} . Instead, the probability distribution spreads toward lower f_{stp} as the travel distance scale increases, especially when $\ell_{surv} \gtrsim 100$ pc.

Figure 9 shows f_{pp} and f_{stp} in $g15784$ at $z=0$ as a function of the three habitability levels, for various damage models and $\ell_{surv} = 100$ pc. From Equations (16)–(17), the panspermia probability is

$$f_{pp}(\mathbf{x}_j) \propto f_{target}(\mathbf{x}_j) \times \sum_i f_{cradle}(\mathbf{x}_i) f_{esc}(\mathbf{x}_i) \mathbb{F}(R_i, R_j, D_{ij}|\ell_{surv}), \quad (22)$$

where

$$\mathbb{F}(R_i, R_j, D_{ij}|\ell_{surv}) \equiv \int_{\ell_{min}}^{\ell_{max}} d\ell F(\ell|R_i, R_j, D_{ij}) w_{damage}\left(\frac{\ell}{\ell_{surv}}\right), \quad (23)$$

with $\mathbb{F}(\dots)$ depending only on the geometry (volumes and relative position) of the source–target star particle pair. Consequently, while

\mathbb{F} may vary from particle to particle, $\sum_i \mathbb{F}$ is mostly determined by the local stellar density around the target star particle. Accordingly, while $\sum_i f_{cradle}(\mathbf{x}_i) f_{esc}(\mathbf{x}_i) \mathbb{F}(\dots)$ is sensitive to both geometry and the baryonic properties of the target star particle, it can be approximated by a function of only R_j in cases where $f_{cradle} f_{esc}$ does not vary much across all relevant source star particles. In other words, if the range of f_{target} in $g15784$ is significantly larger than that of $f_{cradle} f_{esc}$, then $f_{pp} \propto f_{target}$. On the other hand, if the range of f_{target} is similar or narrower than that of $f_{cradle} f_{esc}$, the above approximation cannot be used. As shown in Figures 5 and A4, $0.06 < f_{target} < 0.1$ while $0 < f_{cradle} f_{esc} < 0.1$, even in the noEsc with $f_{esc} = 1$. Consequently, f_{pp} does not correlate clearly with habitability (upper panels of Figure 9). On the other hand, the successful transplantation probability can be written as

$$f_{stp}(\mathbf{x}_i) \propto f_{cradle}(\mathbf{x}_i) f_{esc}(\mathbf{x}_i) \times \sum_j f_{target}(\mathbf{x}_j) \mathbb{F}(R_i, R_j, D_{ij}|\ell_{surv}) \quad (24)$$

and, in a similar way, we can assume that $\{\mathbb{F}\}$ is mostly determined by R_i . Since the range of $f_{cradle} f_{esc}$ is significantly larger than that of f_{target} , we can expect $f_{stp} \propto f_{cradle} f_{esc}$. Indeed, Figure 9 (bottom

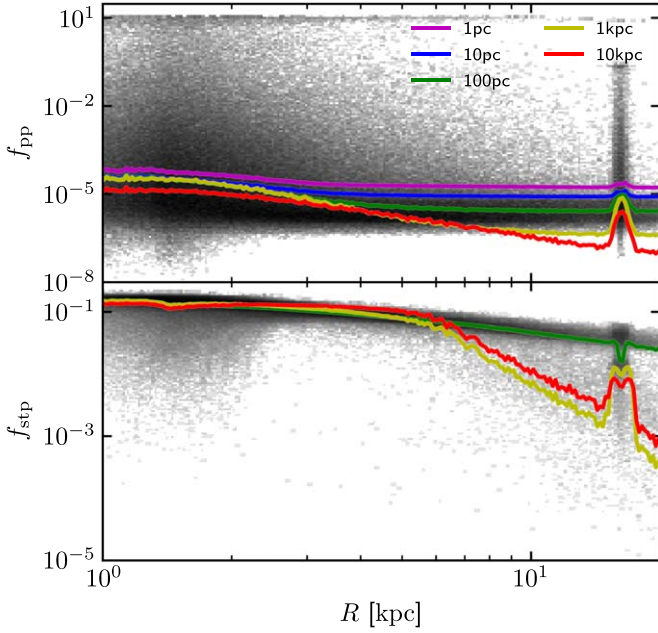


Figure 7. Panspermia probability (f_{pp} ; top) and successful transplantation probability (f_{stp} ; bottom) at $z=0$ in $g15784$ as a function of galactocentric radius. The joint distribution is drawn in a logarithmic scale and in gray scale, assuming exp and $\ell_{\text{surv}} = 100$ pc. On the other hand, the median probabilities for different values of ℓ_{surv} , for the same damage model, are shown by the colored lines.

panels) shows strong correlations between f_{stp} and $f_{\text{cradle}}f_{\text{esc}}$, for different values $f_{stp}/f_{\text{cradle}}f_{\text{esc}}$. Most of the DiskHalo population has high values of both f_{cradle} and f_{stp} ($(f_{\text{cradle}}, f_{stp}) \sim (0.09, 10^{-1})$), while values for CentralDisk, on the other hand, are more widely spread, with a $f_{stp}/f_{\text{esc}}f_{\text{cradle}} \simeq 2$ linear correlation (upper diagonal strip at the bottom panels of Figure 9). Finally, the lower diagonal strips in the bottom panel of Figure 9 correspond to the Spheroids. Interestingly, there appears to be two distinct populations in the $f_{\text{cradle}}-f_{stp}$ plane, with $f_{stp}/f_{\text{esc}}f_{\text{cradle}} \simeq 0.5$ and 0.2, respectively. They disappear when $\ell_{\text{surv}} \geq 10$ kpc, suggesting that they originate from successful panspermia between Spheroids and the main galaxy at low ℓ_{surv} . The strength of correlation between f_{stp} and other two types of habitabilities depends on the correlation between those habitabilities and f_{cradle} —as $f_{\text{target}}(f_{\text{hab}})$ shows a mild (no apparent) correlation with f_{cradle} , so does it with f_{stp} (see Figure 5, for example).

At a fixed value of ℓ , we find that neither the probability and joint distributions of f_{pp} and f_{stp} strongly depend on the damage model (sudden, lin, or exp). While the three damage models have different $w_{\text{damage}}(\ell/\ell_{\text{surv}})$, and therefore different $\mathcal{F}(x_i, x_j)$, the normalization of $f_{pp/stp}$ described above weakens the difference between them. That numerous star particles can affect both f_{pp} and f_{stp} further lessens it. On the other hand, there is significant difference between those three damage models and noEsc, mostly due to differences in escape weight f_{esc} .

5.2. Panspermia Contributions

By definition, both the f_{pp} and f_{stp} of a given star particle are affected by numerous source and target particles. This means that star particles with the same values of f_{pp} or f_{stp} may, however, have a completely different panspermia history. For example, some star particles might have received similar amounts of seeds from numerous particles, while others might have received most of their seeds from only one

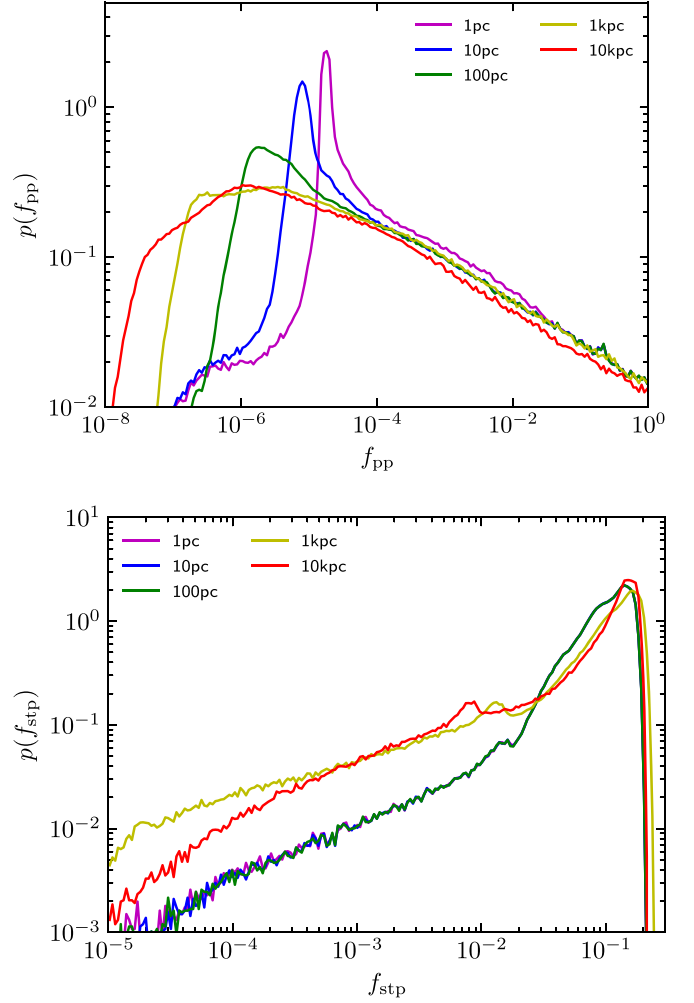


Figure 8. Probability distributions of the panspermia (f_{pp} ; top) and successful transplantation probabilities (f_{stp} ; bottom) in $g15784$ at $z = 0$. Both f_{pp} and f_{stp} are calculated by assuming the exponential damage model (exp) and various travel distance scales (colored lines).

or a few dominant sources. As an attempt to quantify the panspermia history of individual particles, we define the *greatest panspermia contribution* as the highest single f_{pp} or f_{stp} contribution to the sum:¹³

$$\mathcal{F}_{\text{best,pp}}(\mathbf{x}) \equiv \max_{x'} \mathcal{F}(x', \mathbf{x}) \quad (25)$$

$$\mathcal{F}_{\text{best,stp}}(\mathbf{x}) \equiv \max_{x'} \mathcal{F}(x, x'). \quad (26)$$

Both $\mathcal{F}_{\text{best}}$ occupy a narrow range of values and are nearly constant with the galactocentric distance. On the other hand, as shown in Figure 10, their ratios to f_{pp} and f_{stp} show a clear radial trend: $\mathcal{F}_{\text{best}}/f_{pp}$ tends to be high in the DiskHalo, increasing with radius up to values of ~ 1 , and low in both the CentralDisk and Spheroids. This implies that, while in the outer galactic disk and the halo the panspermia probability of a star particle is on average dominated by a single other particle (i.e., a one-to-one transmission), closer to the bulge and in the satellites the f_{pp} of star particles is a sum of contributions

¹³ Ideally, all $\mathcal{F}(x_i, x_j)$ for the entire N_i^2 pairs of possible routes should be considered. However, the large number of $N_* = 746,659$ makes it impractical at the moment. We consider the full list of panspermia contributions and their network in a future work.

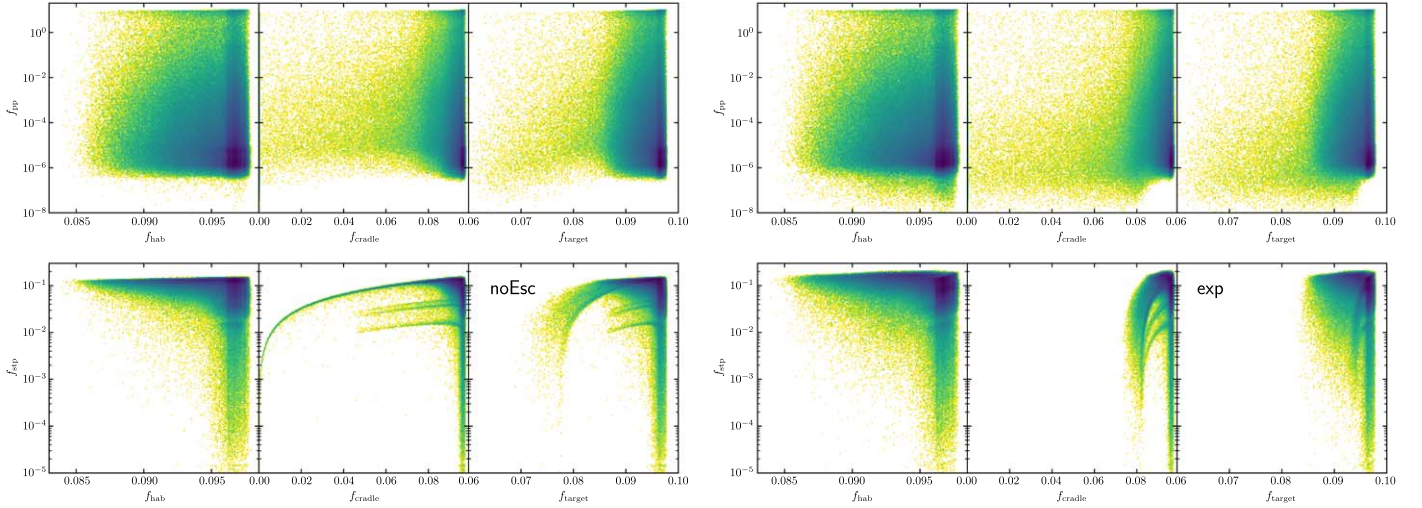


Figure 9. The panspermia (f_{pp} ; top) and successful transplantation (f_{stp} ; bottom) probabilities as a function of three different types of habitabilities (f_{hab} , f_{cradle} , and f_{target}) in $\mathfrak{g}15784$ at $z = 0$. Left: Sudden damage model with $f_{esc} = 1$ for all star particles (noEsc) and $\ell_{surv} = 100$ pc. Right: Exponential damage model (exp) with the same travel distance scale. Both the sudden and lin models give similar results to exp.

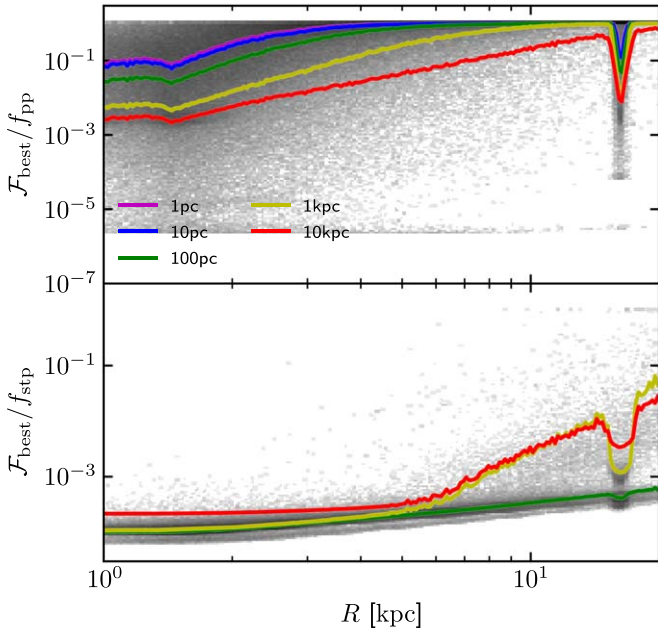


Figure 10. Greatest contribution relative to the panspermia probability, $\mathcal{F}_{best}/f_{pp/stp}$, as a function of galactocentric radius. The colored lines show the median value, as in Figure 7.

from multiple sources. In this case, the high local density more than offsets the lower habitability of particles in these regions. Likewise, $\mathcal{F}_{best}/f_{pp}$ decreases monotonically with increasing ℓ_{surv} , as the larger travel distance allows more source particles to contribute. On the other hand, $\mathcal{F}_{best}/f_{stp}$ is somewhat insensitive to the travel distance until $\ell_{surv} \gtrsim 1$ kpc, when other routes to target particles in the DiskHalo and Spheroids become possible.

5.3. Self-panspermia in $\mathfrak{g}15784$

So far we considered all star particles in our calculation of f_{pp} and f_{stp} , including cases where source and target particles are the same. This possibility of “self-panspermia” accounts for the limited spatial and mass resolutions of MUGS, where each star

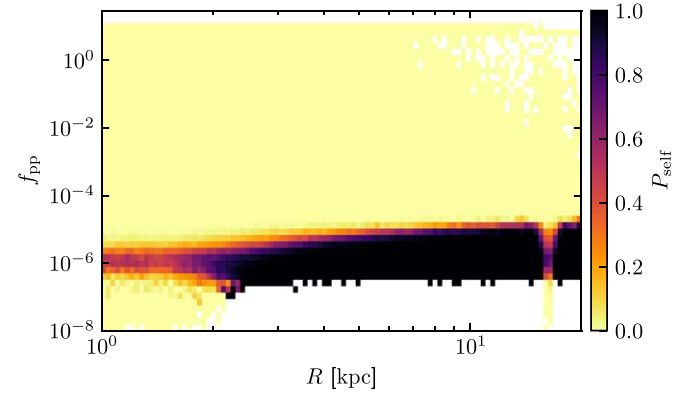


Figure 11. The probability of self-panspermia (P_{self}), where $\mathcal{F}(x, x) > f_{pp/stp}(x)/2$, as a function of R and f_{pp}

particle ($6.3 \times 10^6 M_{\odot}$) contains millions of stars. In this subsection, we investigate the contribution of self-panspermia to the panspermia probability.

We consider that a given star particle undergoes self-panspermia if the panspermia contribution from/to the same star particle is greater than the sum of the contributions from/to the all other star particles, i.e., star particle i undergoes self-panspermia when $\mathcal{F}(x_i, x_i) > f_{pp/stp}(x_i)/2$. Figure 11 shows the distribution of self-panspermia in $\mathfrak{g}15784$ at $z = 0$ as a function of galactocentric radius and f_{pp} , assuming exp with $\ell_{surv} = 100$ pc. Self-panspermia starts to dominate at $R > 2$ kpc, where most of the DiskHalo population exists, and for particles with panspermia probabilities at or below the median value (here $f_{pp} \sim 10^{-5}$). This threshold decreases by 2 orders of magnitude when ℓ_{surv} increases from 1 pc to 10 kpc. Conversely, no self-panspermia occurs in star particles with values of $f_{pp} \gtrsim 10^2$ times greater than the median. On the other hand, star particles at lower galactocentric radii, both in CentralDisk and DiskHalo, tend to undergo less self-panspermia because the high stellar densities near the galactic center may prevent the panspermia process from being governed by a single route. Finally, we find almost no cases of self-panspermia for the successful transplantation probability (f_{stp}), except in the outer, underdense region of the DiskHalo.

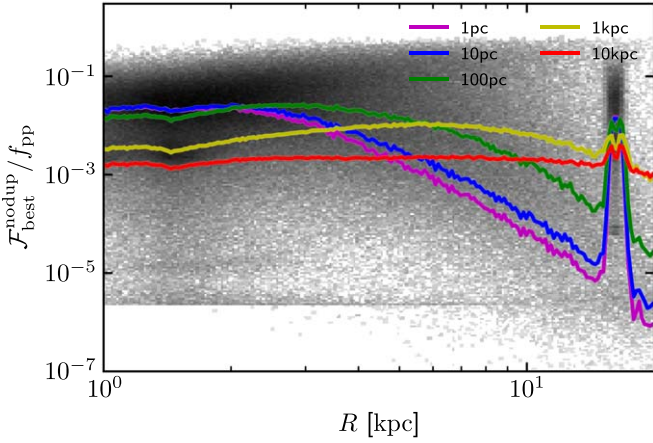


Figure 12. Same as Figure 10 (top), but for $\mathcal{F}_{\text{best}}^{\text{nodup}}/f_{\text{pp}}$, i.e., without the contribution of self-panspermia.

Having estimated self-panspermia, we subtract it from $\mathcal{F}_{\text{best}}$:

$$\mathcal{F}_{\text{best,pp}}^{\text{nodup}}(\mathbf{x}) \equiv \max_{\mathbf{x}' \neq \mathbf{x}} \mathcal{F}(\mathbf{x}', \mathbf{x}) \quad (27)$$

$$\mathcal{F}_{\text{best,stp}}^{\text{nodup}}(\mathbf{x}) \equiv \max_{\mathbf{x}' \neq \mathbf{x}} \mathcal{F}(\mathbf{x}, \mathbf{x}'), \quad (28)$$

with Figure 12 showing the behavior of $\mathcal{F}_{\text{best}}^{\text{nodup}}/f_{\text{pp/stp}}$. Contrary to the full case (Figure 10), $\mathcal{F}_{\text{best}}^{\text{nodup}}/f_{\text{pp}}$ is strongly suppressed at $R > 2$ kpc, in agreement with Figure 11. This implies that, in the `DiskHalo`, most of f_{pp} is self-panspermia, but also that the number of sources contributing to non-self-panspermia increases with galactocentric radius. On the other hand, the latter (i.e., panspermia from other source particles) dominates the `CentralDisk` and `Spheroids`. We also note that, while the fraction of star particles dominated by self-panspermia is large, these tend to have lower values of f_{pp} , as discussed above and therefore contribute less to galactic panspermia.

5.4. Panspermia versus Prebiotic Evolution

In this work we have eschewed a key question that implicitly motivates it, namely: which could be the dominant source of life on habitable planets in the galaxy, in situ evolution or panspermia? Within the methodology used in this paper, assuming that f_{oc} does not depend on, e.g., metallicity and that the timescales of prebiotic evolution and transmission are short compared to the age difference between particles, this could be parameterized proportionally to the ratio between the sums of panspermia probability and of natural habitability. Under these conditions, then, panspermia would take precedence when the habitability of a given particle is lower than the sum of habitabilities of neighboring particles weighted by escape fraction and distance.

In practice, however, since $f_{\text{pp/stp}}$ have to be arbitrarily scaled due to the presence of undetermined parameters, this question cannot be answered quantitatively. The actual, *unnormalized* panspermia probability can be defined as $\hat{f}_{\text{pp,stp}} = \mathcal{R} \times f_{\text{pp,stp}}$, with the true value of \mathcal{R} being unknown. Varying \mathcal{R} for the probability of $\hat{f}_{\text{pp}} > f_{\text{hab}}$ and $\hat{f}_{\text{stp}} > f_{\text{hab}}$, we find that matching the naïve expectation that $P(\mathcal{R}) \simeq \mathcal{R}/(\mathcal{R} + 1)$ would require $\mathcal{R} \gtrsim 10^{3.5}$ and $\mathcal{R} \gtrsim 1$, respectively (for more detail, see Appendix B). Figure 13 shows the radial distribution of star

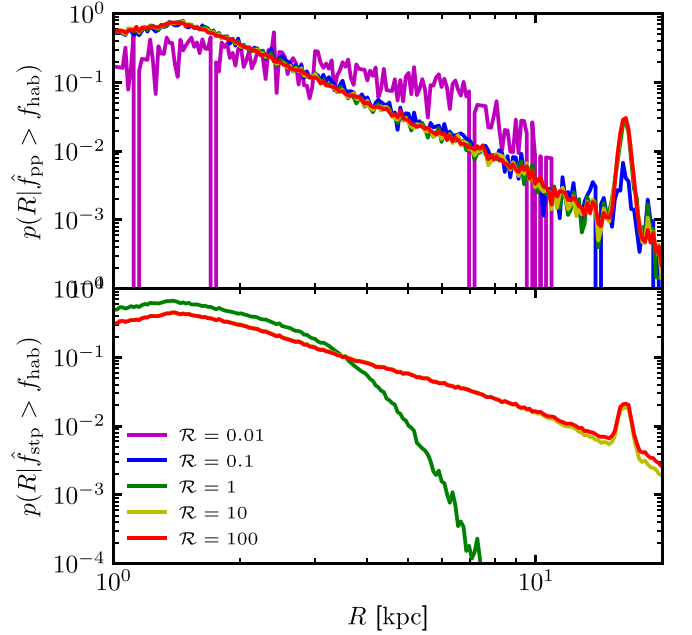


Figure 13. Radial distribution of star particles with unnormalized panspermia probabilities greater than the natural habitability ($p(R|\hat{f}_{\text{pp/stp}} > f_{\text{hab}})$) in $\text{g}15784$ at $z = 0$, for different values of \mathcal{R} . $p(R|\hat{f}_{\text{pp/stp}} > f_{\text{hab}})$ is normalized such that its integral over R is 1.

particles with $\hat{f}_{\text{pp/stp}} > f_{\text{hab}}$ for various values of \mathcal{R} which, for $\mathcal{R} > 10^{-2}$, follows a similar slope to $R-\Sigma_*$ in Figure 2. This confirms that dense regions, such as the `CentralDisk` and inner part of the `DiskHalo`, have a higher chance of being seeded through panspermia.

6. Conclusions

In this paper, we have modeled the probability of panspermia (i.e., of successful material transfer between star systems) and its distribution in Milky Way-like galaxies using a simulated object from the MUGS. To compute panspermia probabilities, we have expanded on the formalism presented in [GH16](#), adding models for the ejection of spores from planets, their escape, transit, and in-transit damage. Our conclusions are summarized as follows:

1. While the median habitability increases with galactocentric radius, the probability for panspermia behaves inversely, being more likely in the central regions of the bulge ($R = 1-4$ kpc), as in the compact dwarf spheroids orbiting the simulated main galaxy. This is mostly due to higher stellar densities, which counterbalances their lower habitability. On the other hand, the panspermia probability is low in the central disk, owing to a lower escape fraction due to metallicity and higher SN rates. In dense regions, many source particles can contribute to panspermia, whereas in the outer disk and halo the panspermia probability is typically dominated by one or, at most, a few source star particles. Unlike natural habitability, whose value varies by only $\sim 5\%$ throughout the galaxy, the panspermia probability has a wide dynamic range of several orders of magnitudes.
2. There is no clear correlation between the panspermia probability and the habitability of the receiving particle, mainly because the former, especially at high values, is

affected by numerous source star particles. On the other hand, it is strongly correlated with the habitability of the source particle, with several distinct stellar populations standing out, corresponding to those in the central disk, outside of the central disk, and in the satellites.

3. Finally, although this cannot be precisely quantified at the moment, we expect the process of panspermia to be significantly less efficient at seeding planets than in situ prebiotic evolution. For example, even in a saturated case where the total panspermia probability is of the order of the total habitability in the galaxy, it would only dominate in 3% of all star particles.

Several caveats remain in our model: first, it includes several factors that we have regarded as unknown constants (e.g., the capture fraction of spores by target planets, the relation between habitability and the presence of life, the typical speed of interstellar objects, and the absolute value of escape fraction of the interstellar organic compounds from source planets). Our results are therefore naturally more qualitative than quantitative. Second, our calculation was done on a single simulation snapshot. That is, it assumes the spatial distribution to be static, while the actual Milky Way rotates and evolves. As such, these results only apply if the typical timescale for panspermia is much shorter than the dynamical timescale of a galaxy. Third, although we have used one of the best mock Milky Way proxies available, some differences exist between the actual Milky Way and $g15784$, which may lead to differences in panspermia probability. For example, our mock galaxy has a larger value of bulge-to-disk light ratio than the actual Milky Way (Brook et al. 2012), and the galactic bulge has been suggested to be well suited for panspermia (e.g., Chen et al. 2018; Balbi et al. 2020). Finally, higher-resolution galaxy simulations with proper implementation of large-scale effects may provide a more realistic estimation of panspermia probability by, among other things, not having to account for self-panspermia (e.g., Crain et al. 2015; Schaye et al. 2015; Lee et al. 2021).

The authors thank Michael Gowanlock and Heeseung Zoe for helpful discussions. We acknowledge Jeremy Bailin, Greg Stinson, Hugh Couchman, and James Wadsley for carrying out the MUGS simulation and allowing us access to the data. S.E.H. was partly supported by the Basic Science Research Program through the National Research Foundation of Korea funded by the Ministry of Education (2018R1A6A1A06024977). S.E.H. was also partly supported by the project 우주거대구조를 이용한 암흑우주 연구 (“Understanding Dark Universe Using Large Scale Structure of the Universe”), funded by the Ministry of Science.

O.N.S. thanks the DIM ACAV+ for postdoctoral funding. The authors acknowledge the Korea Institute for Advanced Study for providing computing resources (KIAS Center for Advanced Computation Linux Cluster System). Computational data were transferred through a high-speed network provided by the Korea Research Environment Open NETwork (KREONET).

Software: IDL, Matplotlib (Hunter 2007), NumPy/SciPy (Virtanen et al. 2020), Pandas (McKinney 2010).

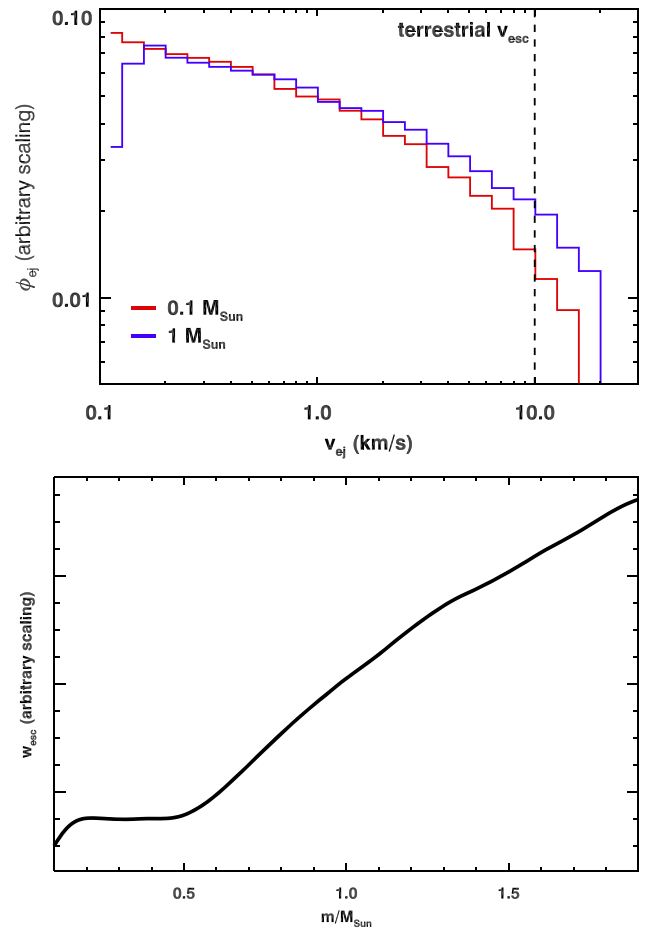


Figure A1. Top: Distribution of ejecta velocities from an impactor population with $f(m) \propto m^{-1.6}$, for a planet within the HZ of a $0.1 M_{\odot}$ (red) and $1 M_{\odot}$ (blue) star, respectively. The dashed vertical line shows the approximate escape velocity of an Earth-mass planet, here set at 10 km s^{-1} for convenience. Bottom: relative fraction of escaping material w_{esc} as a function of host-star mass, assuming that the mass of HZ terrestrial planets does not vary with host-star mass. Only the mass range for which the HZ is defined (Kopparapu et al. 2013) is shown.

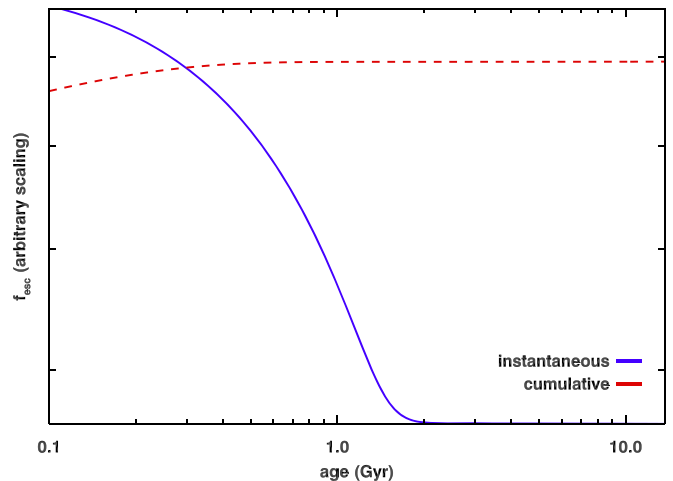


Figure A2. Escape fractions for star particles with a KTG93 IMF, as a function of their age. The solid blue curve shows the instantaneous f_{esc} and the dashed red one shows the cumulative f_{esc} over the lifetime of the star particle.

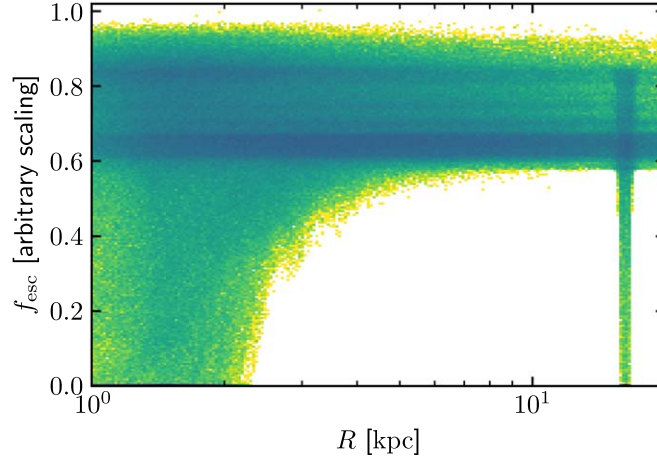


Figure A3. The escape weight (f_{esc}) as a function of galactocentric radius in $\text{g}15784$ at $z = 0$, drawn in a logarithmic scale. Note that the escape weight is shown in arbitrary units.

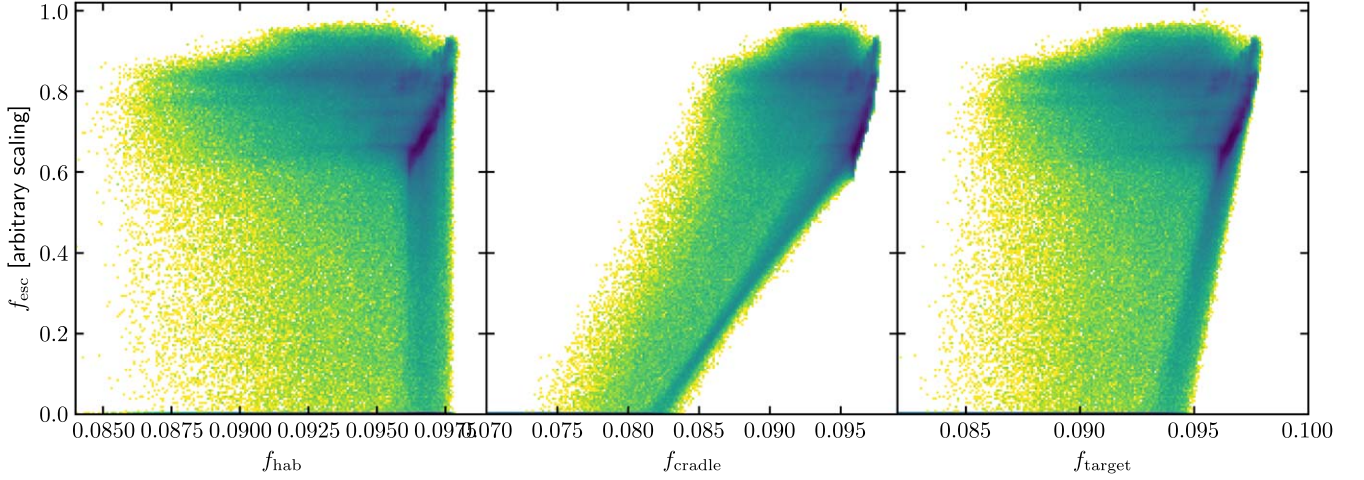


Figure A4. The escape weight (f_{esc}) as a function of three habitability levels (f_{hab} , f_{cradle} , and f_{target}) in $\text{g}15784$ at $z = 0$, drawn in a logarithmic scale.

Appendix A Escape Fractions and Weights

In the case of natural panspermia, we assume that life first develops on the surface of a planet within its star’s HZ, and that spores are then ejected from it by high-velocity impacts. In general, few fragments reach planetary escape velocity and none reach stellar escape velocity. For interstellar panspermia to happen, therefore, the fragments must be accelerated by unspecified processes, which we assume only depend on the host-mass star through its escape velocity within the HZ. Figure A1 shows the distribution of fragment velocities after impact and the (arbitrarily scaled) stellar escape fraction. Figure A2 shows the evolution of the escape fraction w_{esc} over time, assuming that the frequency of impacts follows the one derived from lunar cratering (Neukum & Ivanov 1994):

$$N_{\text{impact}}(t) \propto \exp\left(6.93 \frac{t_{\text{E}} - t}{\text{Gyr}}\right), \quad (\text{A1})$$

where t_{E} the current age of the Earth. Finally, Figure A3 shows the distribution of escape fractions f_{esc} computed for star particles, as a function of their galactocentric distance, and Figure A4 shows their correlation with habitability. A strong correlation exists between f_{esc} and habitability within the

DiskHalo region, whereas star particles in the Central-Disk tend to have lower w_{esc} due to their higher metallicities. Interestingly, rather sharp linear lower boundaries exist in both $f_{\text{cradle}}-f_{\text{esc}}$ and $f_{\text{target}}-f_{\text{esc}}$ parameter spaces, where most of f_{esc} goes to zero at $f_{\text{cradle}} < 0.082$ and $f_{\text{target}} < 0.095$ (Figure A4). Finally, the Spheroids show a radial distribution of f_{esc} similar to that of the main galaxy, though at a smaller scale.

Appendix B Unnormalized Panspermia Probabilities

Figure B5 shows the cumulative probabilities of $f_{\text{pp/stp}}/f_{\text{hab}}$ of $\text{g}15784$ at $z = 0$. In both cases, the overall shape of the probability distribution is similar to those of $f_{\text{pp/stp}}$, mainly due to the narrow range of f_{hab} . Specifically, $P(>f_{\text{pp}}/f_{\text{hab}})$ follows a power-law relation of $P \propto (f_{\text{pp}}/f_{\text{hab}})^{-1/4}$ for $10^{-3} \lesssim f_{\text{pp}}/f_{\text{hab}} \lesssim 10^2$, falling to (nearly) zero for $f_{\text{pp}}/f_{\text{hab}} \gtrsim 10^2$. On the other hand, $P(>f_{\text{stp}}/f_{\text{hab}})$ is nearly zero for $f_{\text{stp}}/f_{\text{hab}} \gtrsim 2$ and plateaus at $P \simeq 0.7$ around $f_{\text{stp}}/f_{\text{hab}} \simeq 0.3$ and 0.01 for $\ell_{\text{surv}} \lesssim 100$ pc and $\gtrsim 100$ pc, respectively. We note that the cumulative probability does not exceed 70% in $\text{g}15784$ because the remaining 30% of star particles have zero habitabilities.

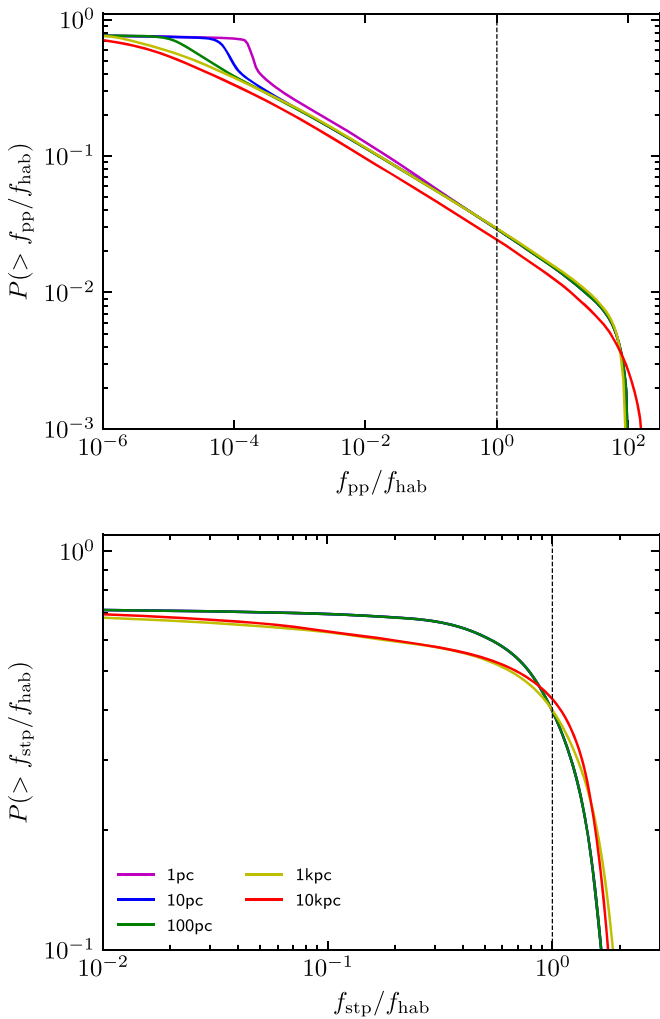


Figure B5. Cumulative probabilities of the ratios between panspermia probabilities ($f_{pp/stp}$) and natural habitability (f_{hab}) in g_{15784} at $z=0$, assuming the `exp` damage model with varying ℓ_{surv} . The dashed vertical line marks $f_{pp/stp} = f_{hab}$. Both f_{pp} and f_{stp} are normalized so that their sum over g_{15784} is same as the sum of f_{hab} .

Table B1

Probability of Star Particles with *Unnormalized* Panspermia Probabilities Greater than Natural Habitability in g_{15784} at $z=0$, for Various Values of \mathcal{R}

\mathcal{R}	$P(\hat{f}_{pp} > f_{hab})$	$P(\hat{f}_{stp} > f_{hab})$
10^{-2}	$\lesssim 0.1\%$	0
10^{-1}	1%	0
10^0	3%	40%
10^1	6%	70%
10^2	10%	70%
10^3	20%	70%
10^4	70%	70%

Table B1 shows probabilities of $\hat{f}_{pp/stp} > f_{hab}$ for various values of \mathcal{R} . The probability of star particles with $\hat{f}_{pp} > f_{hab}$ is much lower than the naïve expectation that $P(\mathcal{R}) \simeq \mathcal{R}/(\mathcal{R} + 1)$. For example, when $\mathcal{R} = 1$, i.e., the total panspermia probability and total habitability is the same, only 3% of star particles have $\hat{f}_{pp} > f_{hab}$, rather than half as would be expected. In fact,

$P(\hat{f}_{pp} > f_{hab}) > 1/2$ occurs only at very high values of $\mathcal{R} \gtrsim 10^{3.5}$. This ensures that only a tiny fraction of star particles dominate the panspermia process of the entire galaxy. On the other hand, $P(\hat{f}_{stp} > f_{hab})$ better matches the naïve expectation for values of $\mathcal{R} \gtrsim 1$.

ORCID iDs

Raphael Gobat <https://orcid.org/0000-0003-0121-6113>
 Sungwook E. Hong (홍성욱) <https://orcid.org/0000-0003-4923-8485>
 Sungryong Hong (홍성용) <https://orcid.org/0000-0001-9991-8222>

References

- Adams, F. C., & Spiegel, D. N. 2005, *AsBio*, 5, 497
 Allen, P. D., Driver, S. P., Graham, A. W., et al. 2006, *MNRAS*, 371, 2
 Anders, P., & Alvensleben, U. Fritze-v. 2003, *A&A*, 401, 1063
 Arrhenius, S., & Borns, H. 1908, *Worlds in the Making: The Evolution of the Universe* (New York: Harper & Brothers)
 Balbi, A., Hami, M., & Kovačević, A. 2020, *Life*, 10, 132
 Brook, C. B., Stinson, G. S., Gibson, B. K., et al. 2012, *MNRAS*, 426, 690
 Bruzual, G., & Charlot, S. 2003, *MNRAS*, 344, 1000
 Burchell, M. 2007, *Proc. SPIE*, 6694, 669416
 Burchell, M. J., Shrine, N. R. G., Mann, J., et al. 2001, *AdSpR*, 28, 707
 Burke, C. J., Christiansen, J. L., Mullally, F., et al. 2015, *ApJ*, 809, 8
 Carroll-Nellenback, J., Frank, A., Wright, J., & Scharf, C. 2019, *AJ*, 158, 117
 Chen, H., Forbes, J. C., & Loeb, A. 2018, *ApJL*, 855, L1
 Collins, G. S., Melosh, H. J., & Marcus, R. A. 2005, *M&PS*, 40, 817
 Crain, R. A., Schaye, J., Bower, R. G., et al. 2015, *MNRAS*, 450, 1937
 Crick, F. H. C., & Orgel, L. E. 1973, *Icar*, 19, 341
 Cumming, A., Butler, R. P., Marcy, G. W., et al. 2008, *PASP*, 120, 531
 Davenport, J. R. A. 2016, *ApJ*, 829, 23
 Dodd, M. S., Papineau, D., Grenne, T., et al. 2017, *Natur*, 543, 60
 Dong, C., Jin, M., Lingam, M., et al. 2018, *PNAS*, 115, 260
 Došović, V., Vukotić, B., & Ćirković, M. M. 2019, *A&A*, 625, A98
 Ferland, G. J., Korista, K. T., Verner, D. A., et al. 1998, *PASP*, 110, 761
 Gibson, B. K., Pilkington, K., Brook, C. B., Stinson, G. S., & Bailin, J. 2013, *A&A*, 554, A47
 Gillon, M., Jehin, E., Lederer, S. M., et al. 2016, *Natur*, 533, 221
 Ginsburg, I., Lingam, M., & Loeb, A. 2018, *ApJL*, 868, L12
 Gladman, B., Dones, L., Levison, H. F., & Burns, J. A. 2005, *AsBio*, 5, 483
 Gobat, R., & Hong, S. E. 2016, *A&A*, 592, A96
 Gonzalez, G., Brownlee, D., & Ward, P. 2001, *Icar*, 152, 185
 Gowanlock, M. G., Patton, D. R., & McConnell, S. M. 2011, *AsBio*, 11, 855
 Grimaldi, C., Lingam, M., & Balbi, A. 2021, *AJ*, 162, 23
 Haldane, J. B. S. 1954, in *New Biology* 16, ed. M. L. Johnson, M. Abercrombie, & G. E. Fogg (Harmondsworth: Penguin), 12
 He, M. Y., Ford, E. B., & Ragozzine, D. 2019, *MNRAS*, 490, 4575
 Higuchi, A., & Kokubo, E. 2019, *MNRAS*, 492, 268
 Horneck, G., Bücker, H., & Reitz, G. 1994, *AdSpR*, 14, 41
 Horneck, G., Rettberg, P., Reitz, G., et al. 2001, *OLEB*, 31, 527
 Housen, K. R., & Holsapple, K. A. 2011, *Icar*, 211, 856
 Hoyle, F., & Wickramasinghe, C. 1978, *Lifecloud: The Origin of Life in the Universe* (London: Dent)
 Hoyle, F., & Wickramasinghe, N. C. 1977, *Natur*, 266, 241
 Hoyle, F., Wickramasinghe, N. C., & Al-Mufti, S. 1986, *EM&P*, 35, 79
 Hoyle, F., Wickramasinghe, N. C., Jansz, E. R., & Jayatissa, P. M. 1983, *Ap&SS*, 95, 227
 Hughes, D. W. 2003, *MNRAS*, 338, 999
 Hunter, J. D. 2007, *CSE*, 9, 90
 Kawaguchi, Y., Yang, Y., Kawashiri, N., et al. 2013, *OLEB*, 43, 411
 Kennicutt, R. C., Jr. 1998, *ApJ*, 498, 541
 Koike, J., Oshima, T., Koike, K. A., et al. 1992, *AdSpR*, 12, 271
 Kopparapu, R. K., Ramirez, R., Kasting, J. F., et al. 2013, *ApJ*, 765, 131
 Krijt, S., Bowling, T. J., Lyons, R. J., & Ciesla, F. J. 2017, *ApJL*, 839, L21
 Kroupa, P., Tout, C. A., & Gilmore, G. 1993, *MNRAS*, 262, 545
 Kruijssen, J. M. D., Pfeffer, J. L., Reina-Campos, M., Crain, R. A., & Bastian, N. 2019, *MNRAS*, 486, 3180
 Lee, J., Shin, J., Snaith, O. N., et al. 2021, *ApJ*, 908, 11

- Li, A., & Draine, B. T. 2001, *ApJ*, **554**, 778
- Licquia, T. C., & Newman, J. A. 2015, *ApJ*, **806**, 96
- Lin, H. W., & Loeb, A. 2015, *ApJL*, **810**, L3
- Lineweaver, C. H., Fenner, Y., & Gibson, B. K. 2004, *Sci*, **303**, 59
- Lingam, M. 2016, *MNRAS*, **455**, 2792
- Lingam, M., & Loeb, A. 2017, *PNAS*, **114**, 6689
- Lingam, M., & Loeb, A. 2018, *AJ*, **156**, 193
- Lingam, M., & Loeb, A. 2021, *Life in the Cosmos: From Biosignatures to Technosignatures* (Cambridge, MA: Harvard Univ. Press)
- Mamajek, E. 2017, *RNAAS*, **1**, 21
- Mastrapa, R. M. E., Glanzberg, H., Head, J. N., Melosh, H. J., & Nicholson, W. L. 2001, *E&PSL*, **189**, 1
- McKinney, W. 2010, in *Proc. of the 9th Python in Science Conf.*, ed. S. van der Walt & J. Millman, 51
- McMillan, P. J. 2011, *MNRAS*, **414**, 2446
- Meech, K. J., Weryk, R., Micheli, M., et al. 2017, *Natur*, **552**, 378
- Melosh, H. J. 1988, *Natur*, **332**, 687
- Melosh, H. J. 2003, *AsBio*, **3**, 207
- Mojzsis, S. J., Arrhenius, G., McKeegan, K. D., et al. 1996, *Natur*, **384**, 55
- Naidu, R. P., Conroy, C., Bonaca, A., et al. 2021, arXiv:2103.03251
- Napier, W. M. 2004, *MNRAS*, **348**, 46
- Neukum, G., & Ivanov, B. A. 1994, in *Hazards Due to Comets and Asteroids*, ed. T. Gehrels, M. S. Matthews, & A. M. Schumann (Tucson, AZ: Univ. Arizona Press), 359
- Nickerson, S., Stinson, G., Couchman, H. M. P., Bailin, J., & Wadsley, J. 2013, *MNRAS*, **429**, 452
- Onofri, S., de la Torre, R., de Vera, J.-P., et al. 2012, *AsBio*, **12**, 508
- Osterbrock, D. E., & Ferland, G. J. 2006, *Astrophysics of Gaseous Nebulae and Active Galactic Nuclei* (Sausalito, CA: Univ. Science Books)
- Pasini, J. L. S., & Price, M. C. 2015, *LPSC*, **46**, 2725
- Petigura, E. A., Marcy, G. W., & Howard, A. W. 2013, *ApJ*, **770**, 69
- Pilkington, K., Few, C. G., Gibson, B. K., et al. 2012, *A&A*, **540**, A56
- Prantzos, N. 2008, *SSRv*, **135**, 313
- Price, M. C., Solscheid, C., Burchell, M. J., et al. 2013, *Icar*, **222**, 263
- Pritchett, C. J., Howell, D. A., & Sullivan, M. 2008, *ApJL*, **683**, L25
- Raskin, C., Scannapieco, E., Rhoads, J., & Della Valle, M. 2009, *ApJ*, **707**, 74
- Sarantopoulou, E., Gomoiu, I., Kollia, Z., & Cefalas, A. C. 2011, *P&SS*, **59**, 63
- Schaye, J., Crain, R. A., Bower, R. G., et al. 2015, *MNRAS*, **446**, 521
- Secker, J., Lepock, J., & Wesson, P. 1994, *Ap&SS*, **219**, 1
- Secker, J., Wesson, P. S., & Lepock, J. R. 1996, *JRASC*, **90**, 184
- Shen, S., Wadsley, J., & Stinson, G. 2010, *MNRAS*, **407**, 1581
- Simon, J. B., Armitage, P. J., Youdin, A. N., & Li, R. 2017, *ApJL*, **847**, L12
- Snaith, O. N., Bailin, J., Gibson, B. K., et al. 2016, *MNRAS*, **456**, 3119
- Spergel, D. N., Bean, R., Doré, O., et al. 2007, *ApJS*, **170**, 377
- Stapleton, O. 1930, *Last and First Men: A Story of the Near and Far Future* (London: Methuen)
- Stewart, K. R., Bullock, J. S., Wechsler, R. H., Maller, A. H., & Zentner, A. R. 2008, *ApJ*, **683**, 597
- Stinson, G., Seth, A., Katz, N., et al. 2006, *MNRAS*, **373**, 1074
- Stinson, G. S., Bailin, J., Couchman, H., et al. 2010, *MNRAS*, **408**, 812
- Stöffer, D., Horneck, G., Ott, S., et al. 2007, *Icar*, **186**, 585
- van Zuilen, M. A., Lepland, A., & Arrhenius, G. 2002, *Natur*, **418**, 627
- Virtanen, P., Gommers, R., Oliphant, T. E., et al. 2020, *NatMe*, **17**, 261
- Wadsley, J. W., Stadel, J., & Quinn, T. 2004, *NewA*, **9**, 137
- Wadsley, J. W., Veeravalli, G., & Couchman, H. M. P. 2008, *MNRAS*, **387**, 427
- Wallis, M. K., & Wickramasinghe, N. C. 2004, *MNRAS*, **348**, 52
- Weber, P., & Greenberg, J. M. 1985, *Natur*, **316**, 403
- Wells, L. E., Armstrong, J. C., & Gonzalez, G. 2003, *Icar*, **162**, 38
- Wesson, P. S. 2010, *SSRv*, **156**, 239
- Wickramasinghe, N. C., & Wickramasinghe, J. T. 2003, *Ap&SS*, **286**, 453
- Yamagishi, A., Kawaguchi, Y., Hashimoto, H., et al. 2018, *AsBio*, **18**, 1369
- Zackrisson, E., Calissendorff, P., González, J., et al. 2016, *ApJ*, **833**, 214
- Zechmeister, M., Dreizler, S., Ribas, I., et al. 2019, *A&A*, **627**, A49